Development and Operation of the Flow Measurement Accuracy Assessment Tool

Mark Christian

A Report Submitted in Fulfillment of the Research

Requirements of the Hydro Research Foundation Fellowship

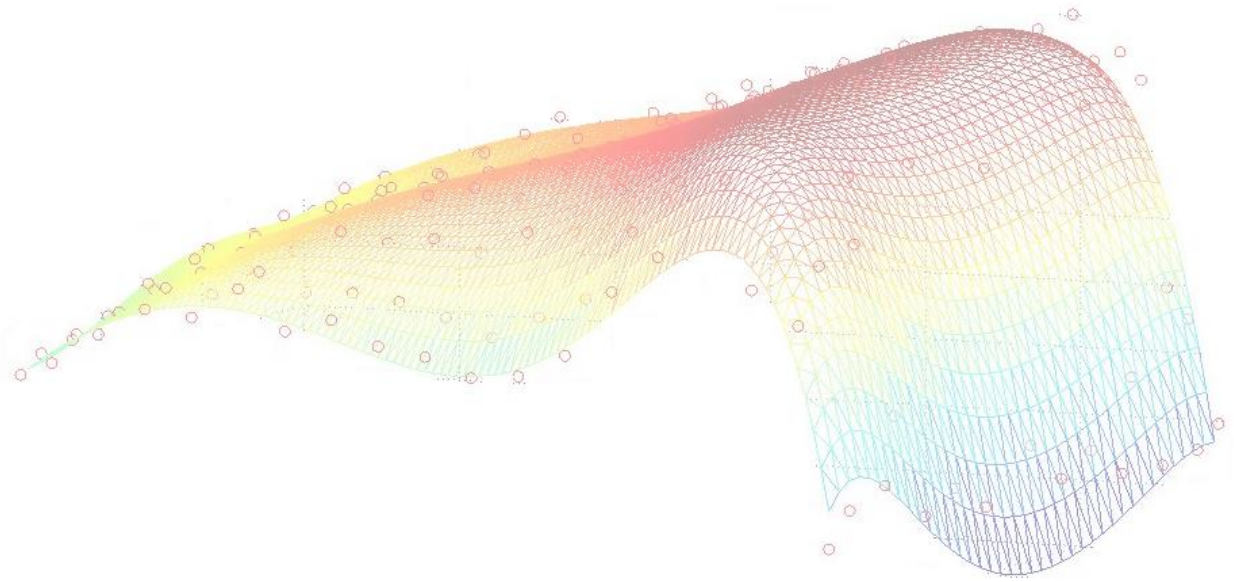

Acknowledgement:

I would like to take this opportunity to express my gratitude to everyone who has supported me over the course of this research project. In particular I would like to thank: my fiancée Guinevere for her boundless encouragement and sincerity; my parents for their love and fostering of my childhood scientific interests; to Brennan Smith, Brenna Vaughn, Deborah Link and Patrick March for their assistance in fostering connections within the hydroelectric industry and invaluable technical and practical advice.

Funding Acknowledgement:

The information, data, or work presented herein was funded in part by the Office of Energy Efficiency and Renewable Energy (EERE), U.S. Department of Energy, under Award Number DE-EE0002668 and the Hydro Research Foundation.

1.0 Abstract

The following report documents the generation of a tool developed by the author over the course of an awarded fellowship by the Hydro Research Foundation. The Appendix of this report contains operational instructions for the use of the tool. The purpose of this tool is to provide the user with an established, rigorous technique to determine the accuracy associated with the application of a user specified number of flow measurement instruments. This tool specifically simulates the application of Current Meters and Acoustic Time of Flight Meters. The tool has been extensively tested and demonstrated consistent operation while being utilized within stated operational constraints. Case studies of both Current Meters and Acoustic Time of Flight Meters demonstrate that the recorded flow rate accuracy changes significantly as a function of: the number of sensors applied; the location of the sensors within the flow path; and overall flow rate itself. Demonstration of this variance acts to validate the need for further research into the effectiveness of flow measurement across the range of hydroelectric facilities given the influence of flow measurement accuracy on plant efficiency and revenue. It should be noted by the reader that the presented work along with the developed tool is preliminarily in nature. Therefore the findings and methodologies developed over the course of this research will be subjected to further peer review via: Oak Ridge National Laboratory Technical Manuscript Report, University of Tennessee Energy Science and Engineering Thesis or Journal Publication. This work is a subsection of the research the author is performing to attain a Doctorate in Energy Science and Engineering at the University of Tennessee which will establish scaling relations between hydroelectric plant characteristics and the value of flow measurement accuracy.

2.0 Motivation

The primary motivation for the development of this tool is to generate a methodology to assess the impact that increasing levels of flow measurement instrumentation has on the accuracy of the recorded flow rate. Currently such a tool does not exist; instead guidance for the application of flow measurement sensors is provided by industry performance test codes such as ASME PTC-18 and IEC 60041. These provide the user with direction as to the appropriate number and type of flow meters to apply (within a range of acceptable geometrical and flow conditions) to achieve flow measurement at a code acceptable level of accuracy. These codes do not, however, address how accuracy of the flow measurement system evolves as the number of sensors ranges from below code acceptability to above. In further research by the author the tool will be used in conjunction with field measurements taken from a wide range of hydroelectric power plants at a variety of flow rates to determine the scaling of flow measurement accuracy based on hydropower plant characteristics. This scaling will then be combined with variations in plant operational styles and the cost of instrumentation to determine the overall scaling factors of the cost benefit curves for hydroelectric plants with a wide range of physical characteristics and operating styles. As will be discussed in the subsequent section, accurate flow measurement has the potential to increase the efficiency of the overall hydroelectric facility, boosting both electrical production and revenue of the facility. These are both important factors given the rise in domestic and international electrical demands in conjunction with increased concerns about the repercussions of producing electricity from carbon-based sources. The overall tool developed by the author is designed to provide hydropower operators with a robust tool to determine the level of flow measurement instrumentation that meets their required Cost-Benefit ratio. Establishment of Cost-Benefit scaling factors is extremely important given the unquantified nature of the benefit received acts as a significant deterrent to the implementation of flow measurement in Hydroelectric Power Plants.

3.0 Role of Flow Measurement

For the importance of accurate flow measurement to be fully understood it is critical to first discuss the role that flow measurement plays in hydroelectric facilities. While there are a myriad of applications of the flow rate, it has three primary roles: confirmation of environmental flow obligations; indication of overall system health; and determination of the optimal application of the individual turbine-generators "units" which comprise the facility. The author's research will primarily address the impact that flow measurement has on the last of these factors; however the developed tool is designed in a broad context such that further research into the impact of flow measurement on the other two primary uses can also utilize this tool. Optimal unit application refers to the use of the unit or series of units which is able to meet electrical generation demand of the facility at the highest possible level of efficiency. The efficiency is measured by comparing the power generated by the unit to the power that could have been generated by an ideal (loss free) unit. Efficiency variation exists, even in units with the same manufacturing characteristics, for many reasons however the leading causes are: variations in the flow profile at the intake which are partially preserved at the location of the turbine; variations the overall health of the system. Subsequently variations in the health of the system is typically be caused by variations in historical operation and environmental conditions between the units. Measurement of individual unit efficiency requires precise knowledge of: Head, Power Production and the Flow Rate. While measurement of these is all susceptible to inaccuracies, flow measurement is widely acknowledged as the most difficult attribute to accurately measure. This is because the flow rate itself cannot be measured directly and must be inferred from a combination measured velocities within the flow and an assumed velocity distribution profile. Accuracy of the flow rate measurement hinges on the corresponding accuracy of the assumed velocity profile and the ability of the sensors to capture the range and distribution of the velocities. The typical velocity distribution is assumed to be an idealized the fully developed flow profile, in the interest of brevity the explanation of fully developed flow has been left to a variety of fluids texts. Conformance with the fully developed profile assumptions is of particular concern when addressing facilities with Quickly Converging Intakes (QCI) as the flow does not have the necessary travel distance to develop fully.

The power generated is combined with the head and flow rate measurement to determine the efficiency of the unit at that specific head and flow rate. This is performed at multiple flow rates to gain as broad of an understanding of the performance of the unit across its electrical production range as possible. A curve is then interpolated across these points to generate the efficiency curve or "characteristic curve" over the generation range of the unit. The characteristic curves of each unit are then evaluated to determine the optimal unit assignment as described above. The purpose of this research is to develop a tool to investigate how the recorded flow rate changes based on the number of applied sensors as variations in the recorded flow rate has the potential to vary the unit application and therefore the overall efficiency of the plant itself.

4.0 Sensor Background

While there are a significant number of sensor systems that can be used to measure flow rates, the Point Current Meter (CM) and Acoustic Time of Flight Meter (ATF) methods have been selected for application. The ATF and CM methods were selected because they are used widely throughout the hydroelectric industry and they operate in three and two dimensions respectively. Operation in varying dimensions was judged to be important, as this provides the user with information as to the impact of

operating in an environment that changes both in two and three dimensions. Operation in this range of dimensions also permits the user to utilize the results of the tool as an analog for other types of flow measurement instrumentation. The following subsections act to provide the reader with fundamental background information about the instruments and the operational characteristics relevant to their application to this tool.

4.1 Point Current Meter Overview

Point Current Meters are instruments which provide the user with point velocity measurements of the flow. There are two fundamental CM designs, those with vertical axis and those with horizontal axis. The vertical axis CM operates inconsistently when encountering axial flows or swirling flows and is therefore not applied to hydropower flow measurement and correspondingly is not considered in this study. The horizontal current meters are typically in the shape of propellers (as seen in Figure 1 (United States Department of the Interior: Bureau of Reclamation, 2001)) which convert the flow of water past the sensor into rotation of the propeller in a predictable manner.

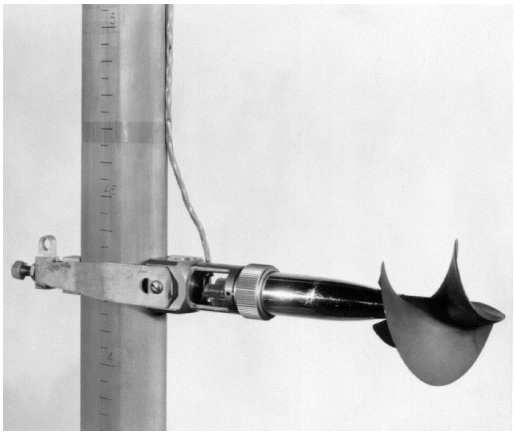

Figure 1: Current Meter

There are two primary methods of application for the CM method: static and transiting. The static method involves mounting a series of CM on a ridged grid within the flow path as seen in Figure 2 (Staubli, 1988) where measurements are recorded simultaneously. The transiting method instead mounts the current meters on a frame as show in Figure 3 (González Salgado, et al., 2013) which is incrementally lowered across the measurement plane; velocities are recorded at the corresponding increments. The transiting method has become increasingly popular because it requires significantly fewer sensors however application of this method is constrained to locations capable of accommodating the frame. This is typically in the intake gate slots of the plant; however at these locations the flow is not fully developed. Additionally the frame can easily be moved from one intake to another, allowing a single frame to be used to measure the flow of an entire plant. Conversely while the static system requires significantly more effort to install and a larger number of sensors it has the advantage of being applicable to a higher number of points within the flow path. Additionally given that the measurements are taken simultaneously this method is applicable to the measurement of highly transient flows.

An area that must be addressed in regards to the CM method is increased flow rate that this technique introduces. The current meters and mounting frame act as a constriction within the flow path; and in order to preserve the flow rate an increase in the velocity corresponding to the reduced cross sectional

area of the conduit is observed. As the simulated sensors are ideal, their impact is assumed to be negligible; and therefore it is important for the user to ensure that the data analyzed with this tool is not influenced by the method used to record it.

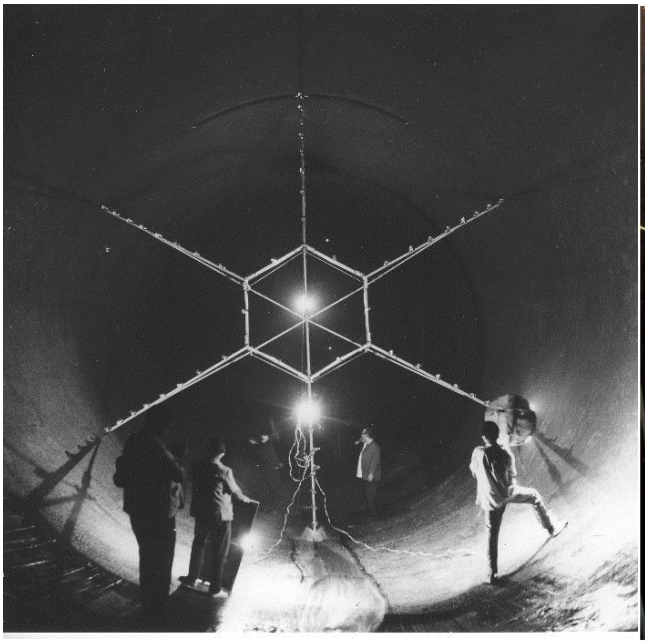

Figure 2: Grid Mounted CM

Figure 3: Transiting CM

4.2 Acoustic Time of Flight

The Acoustic Time of Flight (Figure 4 (Rittmeyer, 2014)) flow measurement method utilizes the impact of the bulk fluid velocity on the transit time of an acoustic pulse traveling upstream and downstream to determine the flow rate along the path of the pulse. The AFT system is comprised of a pair of acoustic transducers in a configuration as demonstrated in Figure 5. The ATF sensors measure the flow utilizing two discrete steps. Initially the upstream transducer produces an acoustic pulse directed downstream, and the movement of the water acts to actually slightly increase the velocity of the acoustic pulse reducing the transit time of the pulse. Once this initial pulse has been received the downstream transducer produces an acoustic pulse directed to the upstream transducer and the bulk flow of the water acts to slow down the pulse and therefore increase the transit time of the pulse. This differential in transit time is combined with the length of the acoustic path to determine the average flow rate along this transect. Whereas the CM system in essence records discrete point velocities within the flow, the AFT system records the average velocity of the flow along this transect, therefore operating in three dimensional space.

Figure 4: ATF Sensor

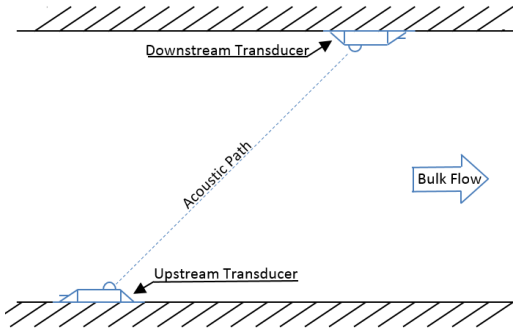

Figure 5: ATF Sensor Layout

The mechanism of mounting the ATF system is primarily dependent on the conduit where the ATF system is applied. Ideally the ATF system is located on an exposed section of conduit where it is mounted by drilling holes into the conduit from the exterior allowing for the transducer section of the sensor to be inserted into the conduit, leaving the remainder of the instrument on the exterior of the conduit as shown in Figure 6 (Gruber & Peter, 2010). In the case where the conduit is not exposed or it is not feasible to drill through the conduit the AFT system must be mounted entirely on the interior of the conduit. The signal from the instrumentation must be transmitted via cable to location where it is feasible to drill through the conduit, allowing the cable to exit the conduit (see Figure 7 (Gruber & Peter, 2010)).

Figure 6: Externally Mounted ATF

Figure 7: Internally Mounted ATF

As with the CM method there is an area that must be addressed in the application of the ATF system. This is the impact of flows not in the direction of the primary flow, referred to as skew flows. The skew flows impact the measured velocity because the acoustic pulse travels in all three dimensions and therefore skew flows act to alter the transit time of the acoustic pulse similarly to the primary flow. Typically these are assumed to be of negligible impact however this assumption is valid only when the flow path where the ATF system is mounted falls within hydraulic constraints. The impact of skew flow in one direction can be compensated for with the application of an additional acoustic path in the opposite direction in the same plane as the skew flow that is being compensated for as demonstrated in Figure 8. It should be noted for however this will not compensate for skew flows in the third dimension, and the application of an additional path will not compensate for its influence.

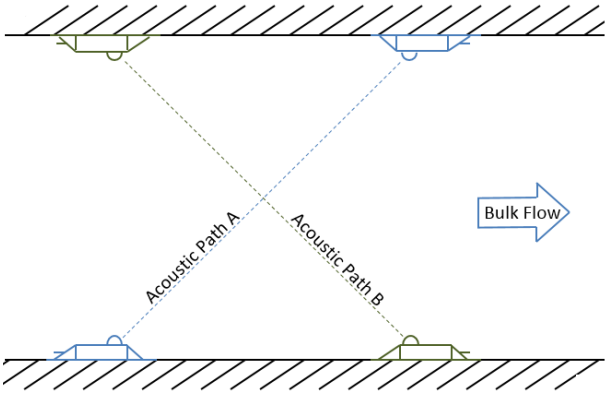

Figure 8: Double Path ATF

5.0 Regression Methodology

The following section is designed to act as an overview of the numeric method and the assumptions associated with the numerical regression technique utilized in this tool. The regression technique is an integral component of this tool as it allows for the reasonable prediction of the flow rate at locations other than those measured within the flow. The Least Squares Approximation (LSA) numerical method technique is used rather than a Kriging or Cubic Spline technique because it is desirable to generate a continuous function of a scalable order. Further research may include the application of a Spline or Kriging methodology to act to confirm the validity of the results generated by the LSA method.

5.1 Fundamental Numerical Assumptions

The LSA method at assumes that the data provided is a function of a polynomial of a user selected order whose coefficients are calculated to minimize the variance between the measured velocities. When single dimensionality is assumed, the velocity at each point is assumed to be of the form of Equation [1]. From this, the coefficients are solved for by utilizing a Gauss solution technique on Equation [2], generated from the values found in Equation [1]. Where: c_n refers to coefficients of the polynomial that are being solved for; U_x is the velocity at the point x; and N is the number of data points that are provided.

$$U_x = c_0 + c_1 x + c_2 x^2 + \cdots + c_n x^n \qquad [1]$$

$$\begin{bmatrix} N & \sum_i^N x_i & \sum_i^N {x_i}^2 & .. & \sum_i^N {x_i}^n \\ \sum_i^N x_i & \sum_i^N {x_i}^2 & \sum_i^N {x_i}^3 & .. & \sum_i^N {x_i}^{n+1} \\ \vdots & \vdots & \vdots & & \vdots \\ \sum_i^N {x_i}^n & \sum_i^N {x_i}^{n+1} & \sum_i^N {x_i}^{n+2} & .. & \sum_i^N {x_i}^{2n} \end{bmatrix} \begin{bmatrix} c_0 \\ c_1 \\ \vdots \\ c_n \end{bmatrix} = \begin{bmatrix} \sum_i^N U_i x_i \\ \sum_i^N U_i {x_i}^2 \\ \vdots \\ \sum_i^N U_i {x_i}^n \end{bmatrix} \qquad [2]$$

The author converted this methodology to two and three dimensional regressions for the CM and ATF meters respectively. The tool is designed to determine polynomial coefficients which minimize the variation between the supplied data and the predicted value at that point. As such it should be noted that the function calculated will not precisely represent the distribution, rather it is designed to represent the overall distribution of the flow. Minor inaccuracies are considered to be permissible given both that there is permissible uncertainty in the flow meters themselves and also that the purpose of this work as it applies to the author's thesis is to determine how the accuracy of the flow meters changes rather than precisely measure the flow itself. Increased accuracy can be obtained by increasing the order of the polynomial to which the data is fit, a factor which is specified by the user in both two and three dimensional regression codes. It should be noted, however when utilizing this tool that while increasing the order of the polynomial will reduce the variation between the provided data set and the function. Eventually this will also result in the polynomial will become increasingly oscillatory as the polynomial increasingly attempts to conform more completely to the provided data set. This is known as Runge's Phenomenon (Fornberg & Zuev, 2007) and can be observed in Figures 9 and 10 which represent the polynomial regression of a 6^{th} and 11^{th} order respectively. The higher order function achieves a lower variation between the polynomial prediction and the actual dataset; however it can be observed that the velocity distribution is much more likely to align with the prediction of the lower order fit.

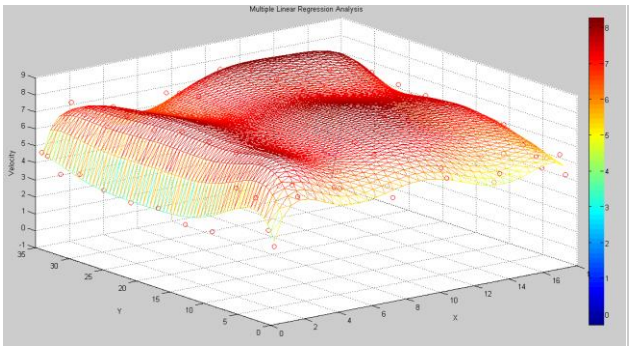

Figure 9: 6th Order Regression

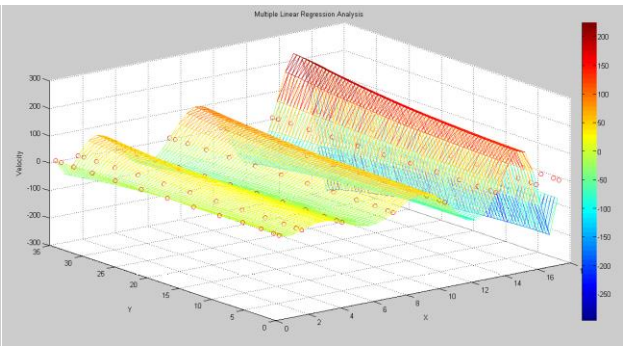

Figure 10: 11th Order Regression

As user judgment is considered the best method to determine the appropriateness of the polynomial fit the tool is designed to allow the user to select the order of the polynomial that will be fit. Figure 11 below demonstrates the impact of the order of the polynomial regression on the simulated ATF sensors. While the method of simulation will be described in the appropriate section below, it can be seen that as the order of the polynomial regression increases the level of resolution of the flow rate correspondingly increases, resulting in increasingly accurate sensor simulation. The actual procedure for this selection is included in the Operation Appendix found below; however this provides the user with an interesting opportunity perform an investigation as to the impact of the order of the polynomial regression on the predicted accuracy increase from the application of additional sensors.

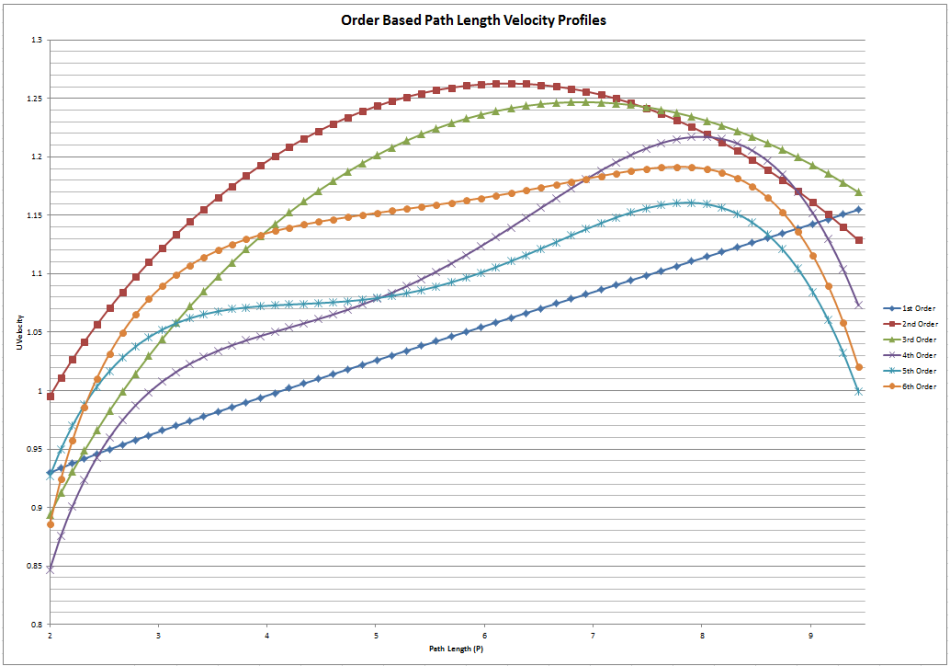

Figure 11: Impact of Regression Order

5.2 Application to Point Current Meters

The idealized current meters are assumed to operate in a single plain and therefore a two dimensional regression solution is utilized to represent the distribution of the flow across the plain. The polynomial function is assumed to take the form of Equation 3 where: U is the velocity; n is the order of the polynomial; and x and y are the breath and width of the measurement plain as is shown in Figure [12]

$$U = c_0 + c_1 x + c_2 y + c_3 x^2 + c_4 xy + c_5 y^2 + \cdots + c_{n-1} xy^{n-1} + c_n y^n \quad [3]$$

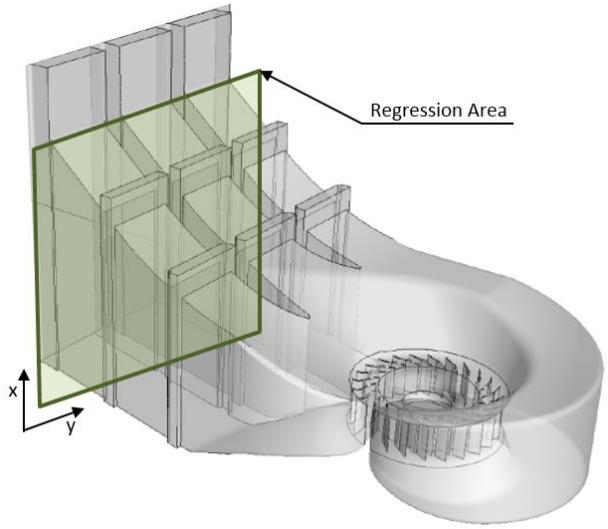

Figure 12: 2D Regression Area

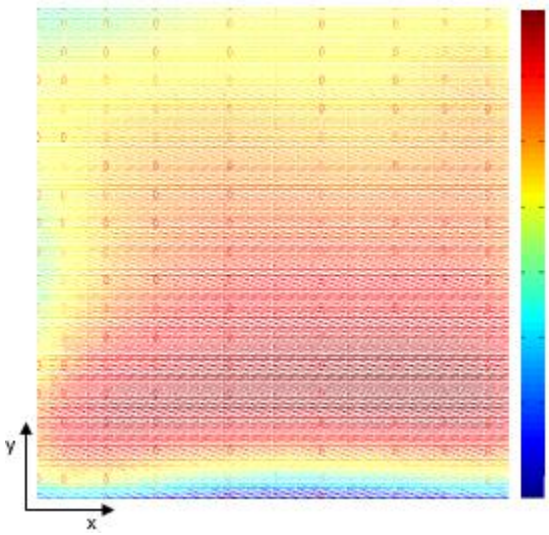

Figure 13: Sample Regression Velocity Distribution

It should be noted that the 2 dimensional LSA regression code developed for this tool will always generate a function for a rectangular space, where the maximum and minimum of each dimension represent the boundaries of the interpolation zone. Due to this the reader should take appropriate steps within the sensor simulation if the conduit possesses a non-rectangular conduit. Additionally it is important for the reader to fully understand the differentiation between interpolation and extrapolation, as interpolation is typically significantly more accurate than extrapolation. Interpolation is the process of approximating the values located in the interval between two known values whereas extrapolation uses the trends of the known data set to approximate values outside of the bounds dataset itself. The extrapolation typically becomes increasingly inaccurate as the distance from the known values increases in combination with the variability of the values themselves. As such it is recommended that user of this tool minimizes the use of extrapolation capability of the tool. Ideally extrapolation should only be utilized to approximate the (minimal) region of the flow between the conduit wall and outmost set of sensors.

4.3 Application to Acoustic Time of Flight Meters

As described above the ATF system operates in three dimensions and therefore an applicable regression code must generate a distribution of the velocity in three dimensions as shown in Equation [4]. Similar to before U is the velocity; n is the order of the polynomial; however in this case y, z and x are the breath, height and streamwise distance of the conduit respectively as shown in Figure 14.

$$U = c_0 + c_1 x + c_2 y + c_3 z + c_4 zx + c_5 x^2 + c_6 xy + c_7 y^2 + c_8 yz + c_9 z^2 + \cdots + c_{n-1} xy^2 z^{n-1} + c_n xyz^n \quad [4]$$

As with the 2D regression, the 3D regression generates a function between the maximum and minimum of each dimension of the values provided such as those in Figures 14 and 15. This is of particular concern in non-regular conduits as non-realistic extrapolation will occur outside of the conduit in the region between the bounds of the regression area and the conduit itself as shown. A method to compensation for this will be discussed further in the sensor simulation section.

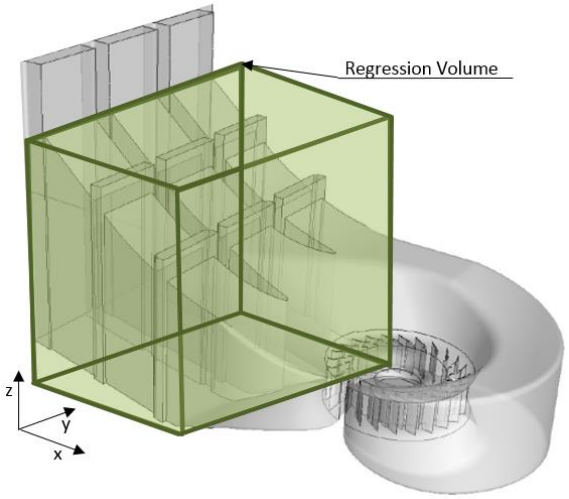

Figure 14: 3D Regression Volume

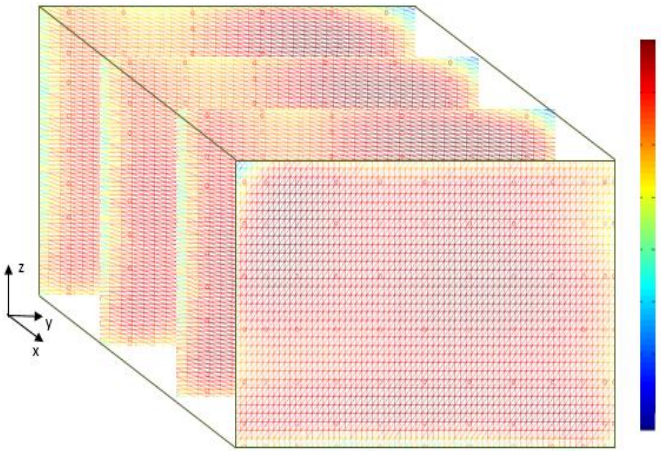

Figure 15: Sample Regression Velocity Distribution

6.0 Sensor Simulation

The following section is designed to provide the user with insight into the process in which the flow measurement sensors are simulated. This allows the user of this tool to fully understand the method and assumptions in which the flow distribution used to assess what velocities the individual sensors would record. The simulated sensors are used at increasing densities to assess the overall flow rate. The predicted flow rate produced by each sensor density is then compared to the known flow rate as determined by an integration of the regressed flow distribution polynomial.

6.1 Point Current Meters

Simulation of the CM sensors benefits from the assumption that the sensors themselves measure point velocities within the flow path. As such simulation of these sensors simply requires that the appropriate values of x and y are imputed into the velocity function and the velocity is recorded.

6.2 Acoustic Time of Flight Meters

Simulation of the ATF method requires significantly more effort than the CM method as the sensors themselves detect the mean velocity of the fluid flow along the acoustic pulse. This requires an integration of the fluid velocity along the path of the acoustic pulse itself; as such this correspondingly requires that the fluid velocity be converted from a function of the Cartesian coordinates to that of a path length, P, as shown in Figure 16.

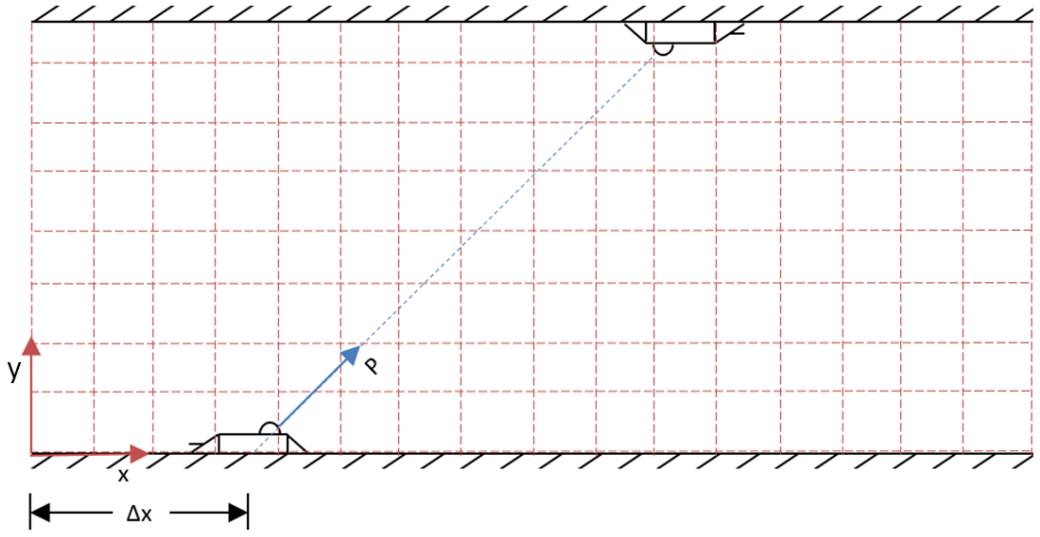

Figure 16: Conversion from Cartesian to Linear Coordinates

Given the size of the polynomial two simplifying assumptions were made; the first was that the acoustic pulse would be set at a constant vertical location, and the second was that the acoustic pulse would be directed across the flow path at a 45 degree angle. These two assumptions make it possible to convert Function [2] to a useable form using Functions [5] through [7]. Future work on this tool will allow for the sensor to be simulated at both varying angles and in three dimensions. As described in the ATF background section additional meters can be used across the flow path (known as cross path) remove the influence of skew flow. Given this, the velocity measured by the single path sensor is calculated by Equation [8] whereas the double path is assumed to be of the function [9] as the cross path is removes the influence of the skew flow, V.

$$P = \sqrt{(x + \Delta x)^2 + y^2} \quad [5]$$

$$x = \sqrt{\frac{P^2 - 2\Delta x^2}{2}} \quad [6]$$

$$y = \left[\sqrt{\frac{P^2 - 2\Delta x^2}{2}} - \Delta x\right] \quad [7]$$

$$U = \frac{1}{P_2 - P_1}\int_{P_1}^{P_2} U(P) + V(P)\, dP \quad [8]$$

$$U = \frac{1}{P_2 - P_1}\int_{P_1}^{P_2} U(P)\, dP \quad [9]$$

6.3 Layout Assumptions

The following section addresses the assumptions that are used by the tool both in regards to placement of the sensors and the method utilized to relate the determined velocities to the overall flow rate. It should be noted by the reader that these two factors have significant impact on the accuracy of the determined flow rate. There exist many different numerical methods to convert the measured velocities to an overall flow rate, however given the initial nature of this tool the decision was made to use a basic equal area-weighting technique. This technique divides the area into equal areas with a sensor located at the middle of each and the recorded flow is assigned to the entirety of the area. The rational for this is that other numerical methods make assumptions about the distribution of the flow, which may or may not be accurate. Addition of the code dictated numerical method represent additional work that will be performed and will be discussed is the subsequent sections.

6.3.1 Current Meters

The CM sensors are assumed to be distributed using Equations [10] and [11] for the locations in reference to conduit width (W) and height (H) respectively. It should be noted that the tool assumes that the number of sensors (n) increases exponentially. It should be further noted that the distribution, k and j refer to the horizontal and vertical grid distribution at which the sensors are placed at the gridline intersections. As described above the area-weight method calculates the overall flow rate using Equation [12]. Further work will adopt a log-linear sensor placement strategy and weighting function as recommended by industry code, however accurate application of this method requires mapping of the traditional distribution in a circular cross section into a rectangular cross section.

$$Y_{k,i} = \frac{W}{\sqrt{n} + 1} i \quad [10]$$

$$Z_{j,i} = \frac{H}{\sqrt{n} + 1} i \quad [11]$$

$$Q = \sum_{i}^{n} U_{jk} \frac{HW}{n}$$

[12]

6.3.2 Acoustic Time of Flight

The ATF sensor placement also utilizes a basic equal weight distribution methodology where the sensors are placed at a depth (Z_i) into the conduit, according to Equation [13] and the overall flow rate (Q) is determined by Equation [14] where: H is the height of the conduit; L is the width of the conduit; n is the number of sensors; i is the individual sensor. As with the CM method an increase in the number of sensors acts to increase the recorded resolution of the overall flow rate. In future work the author will include the code recommended Gauss-Legendre Quadrature method into this tool which will determine both the location of the sensors and the method in which the flow rate is determined from individual velocities.

$$Z_i = \frac{H}{n+1} i$$

[13]

$$Q = \sum_{i}^{n} U_i \frac{HW}{n}$$

[14]

7. Case Studies

The following section is provided to demonstrate the results of the application of this tool to a hydroelectric facility. In the case of the Current Meter simulation, actual field data collected from a unit acceptance test was available and therefore this data was used. This same level of information is not available in three dimensions because the implementation of point velocity sensors in three dimensions within a hydroelectric conduit at a density required to gain meaningful insight into the flow distribution is logistically and economically infeasible. Therefore the Acoustic Time of Flight Simulation utilizes the results of a high density Computational Fluid Dynamic (CFD) model of a QCI provided by the Pacific Northwest National Laboratory.

7.1 Point Current Meter

The current meter simulation modeled a high head unit with three intake bays, all of which were modeled. Fortunately the data provided included the flow distributions of four different flow rates (also known as Runs), allowing for an investigation into the change in sensor performance corresponding to variations in the flow rate. The ability to perform such a study is of particular importance because this allows the user of the tool to anticipate, to a higher level of accuracy, the change in accuracy of the unit characteristics across the operational range of the unit. Figure 17 visualizes the extent to which the flow distribution changes both as a function of the intake bay and the flow rate.

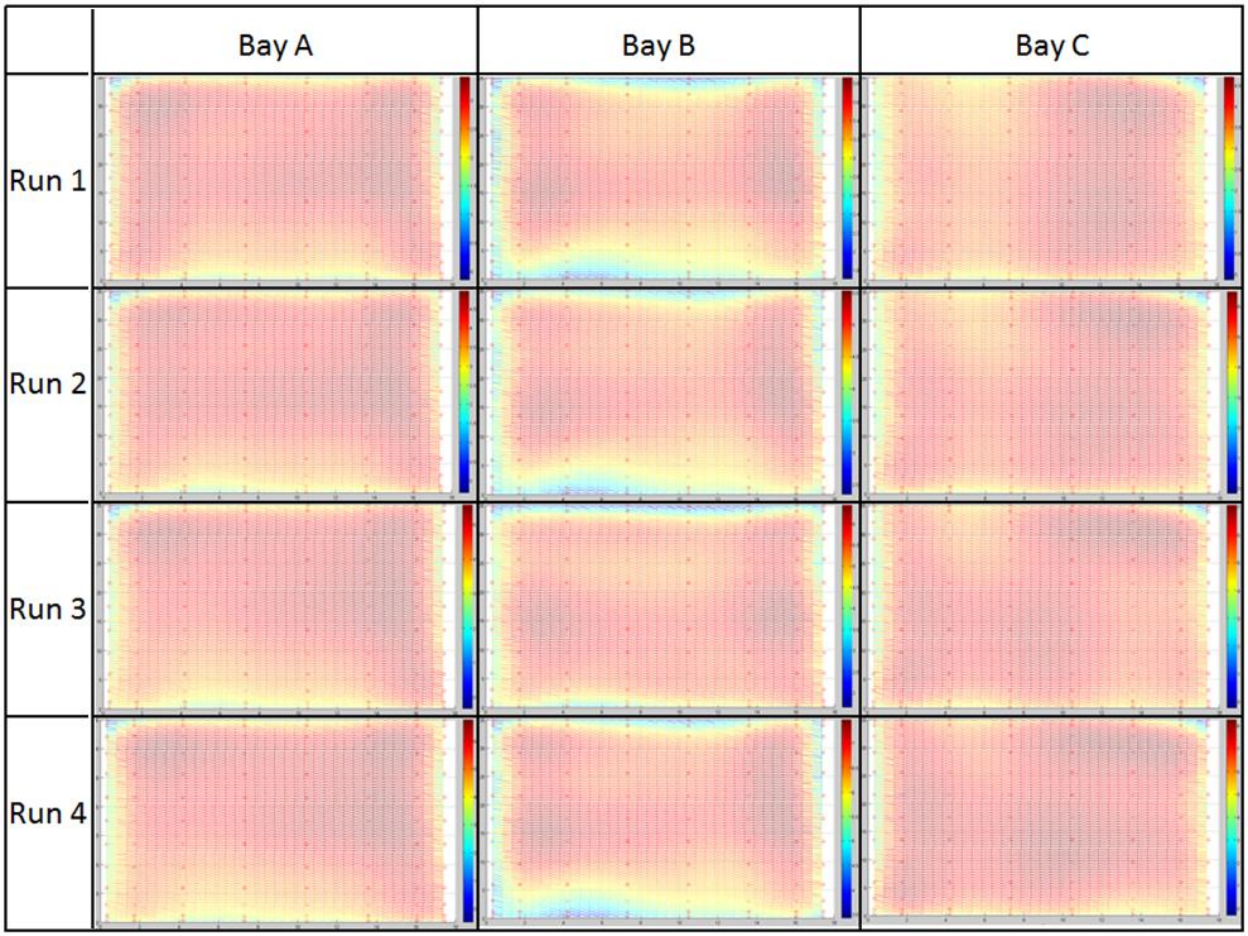

Figure 17: CM Case Study Velocity Distribution

All twelve of the flow distributions were analyzed using the 2 dimensional regressions Matlab code and CM simulation Excel tool that were developed over the course of the research. These tools provided the author with the overall flow rate would be recorded by sensors at the specified quantities at each of the flow rates. The subsequent analysis of the predicted flow data provided the author with several intriguing results. The first of which is the variation between the flow rate predicted by sensors at varying densities. As the tool simulates fourteen different numbers of sensors, the performance of: 25, 64, 100, and 144 sensors along with the true flow rate in Bay A displayed in Figure 18. An area that should be noted in this Figure however is that even at the highest number of applied sensors a large differential exists between the actual and recorded flow rates (an average of 6.14 percent). This indicates two things to the author: that the overall flow distribution is highly variable and that additional work should be performed on the CM simulation section. In regards to the simulation of the sensors it is evident that the capability to simulate sensors at a higher density should be added to capture the full range of the accuracy evolution. Regardless of this it can be observed that at all levels of flow measurement density the flow rate is actually over predicted, albeit to extents varying based on the number of sensors. As mentioned above, one of the primary uses of flow measurement data is to determine the efficiency of the units comprising the plant itself. It is important to note that an over prediction of the flow rate corresponds to an under prediction of unit efficiency as it assumes that more fuel is provided to the turbine than actually is. While not graphically displayed, Bays B and C

demonstrated similar over prediction of the flow rate with an average error of 4.65 and 5.45 percent respectively at the highest number of simulated CM. The numerical results of these Bays are provided in Section 9.1 below.

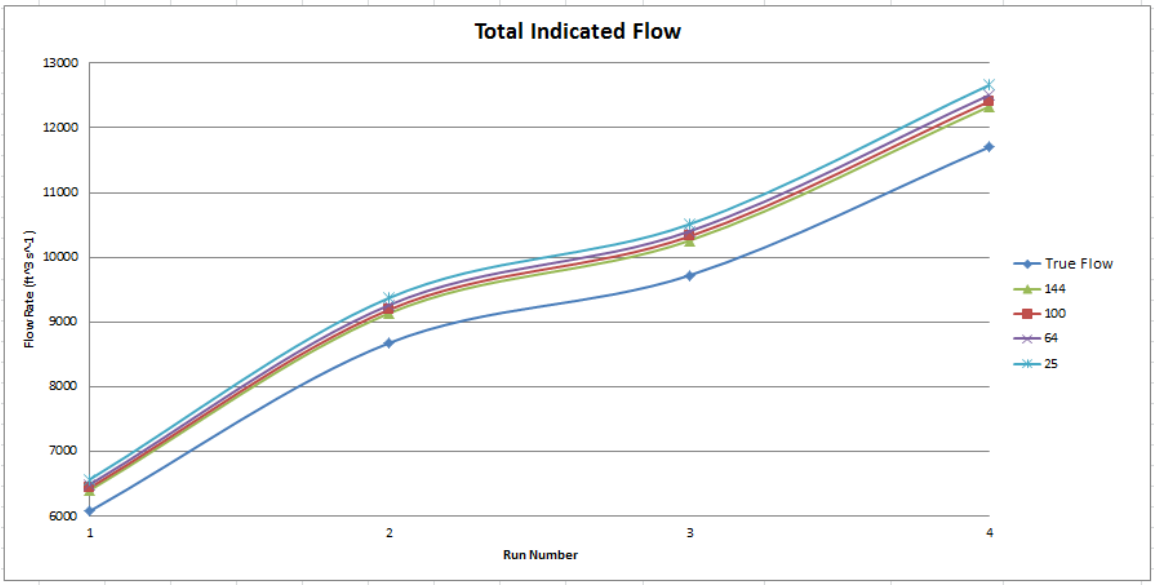

Figure 18: Bay A CM Indicated Flow

Another interesting result of this case study is the distribution of the flow between the Bays as shown in Figure 19. Bay C consistently has the highest flow rate of the intakes with the distribution of the flow being 28.72, 33.85, and 37.43 ft^3sec^{-1} on average for Bays A, B and C respectively. Limitations on information about the geometry of the intake prohibits the author from making an informed estimation as to the reason for this distribution of the flow however it is speculated that the intake is similar to that in the AFT simulation case study below. If this is correct, then the geometry of the intake acts to distribute the water. Naturally this topic is discussed more extensively in the following section. The increased information about the flow distribution and accuracy provided by this tool prompts an interesting operational decision that must be made by the operator about the level of appropriate flow measurement. As discussed Bay A represents the lowest average flow rate however it also represents the highest error. Correspondingly the operator must decide whether more accurately capturing the flow rate in Bay A is worth investing in flow meters beyond the level required for accurate measurement of Bays B and C.

Finally, an important attribute of the case study was the demonstration of the role of the flow rate in the increase in accuracy provided by a larger number of sensors. Figure 20 demonstrates the ability of four levels CM density to accurately predict the overall flow rate along with the differentials between the accuracy levels. It can be observed from this data that the differential in increased accuracy achieved by increasing the number of sensors ranges from an average maximum of 0.086 to 0.005 percent across flow rates. While the variation may not appear to be significant its presence should indicate the importance of taking into account the non-linearity of increases in flow measurement accuracy across flow rates.

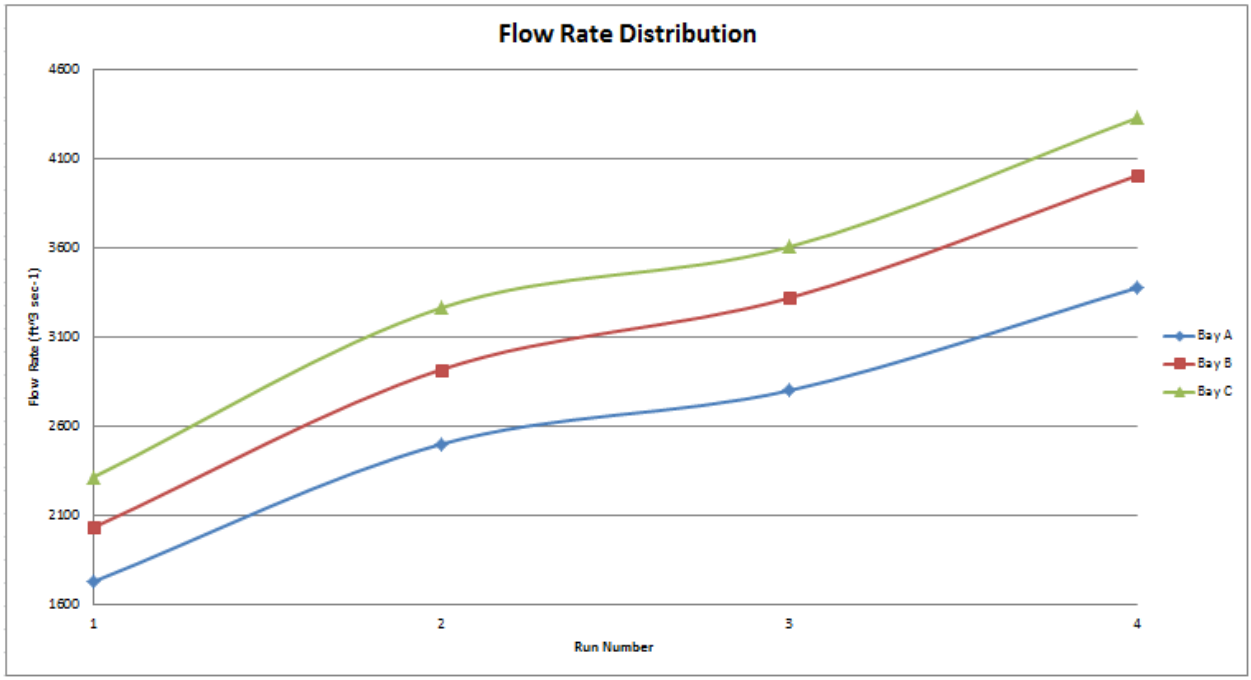

Figure 19: Bay Flow Rate Distribution

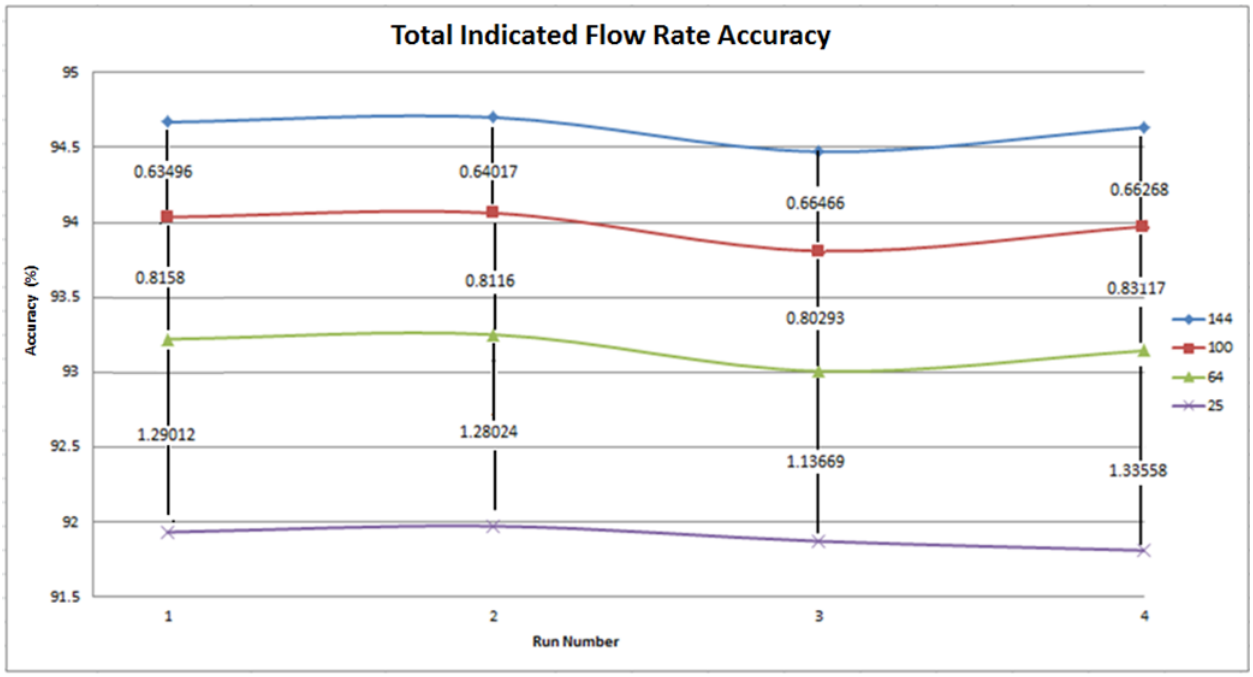

Figure 20: Variations in CM Sensor Accuracy

7.2 Acoustic Time of Flight Meters

As mentioned above the AFT case study only contains a single velocity distribution data for a CFD model of a single flow rate of a QCI. Due to this fact of this there are several considerations that must be taken into account. The first is that rather than investigating how the flow rate sensors perform at varying flow rates, this case study will instead focus on the change in accuracy that occurs as sensors are simulated at

varying locations along the flow path. This information is of particular interest for the ATF system as this method is traditionally mounted in the walls and is applied for an extended period therefore its application would not be restricted to the gate slot as the CM typically is. Given this range of locational applicability such an investigation is important. The second factor that must be taken into account is the fact that rather than using actual field data, this case study utilizes CFD modeled data, and therefore the accuracy of the results is tightly linked to the accuracy of the modeled system. Of particular concern for this is setting boundary conditions representative of those that are actually present in a physical system (Almquist, Taylor, & Walsh, 2011). Variations from the realistic boundary conditions will result in inaccurate flow rate distribution and therefore care must be taken when utilizing exclusively CFD results in significant investments. Finally as the tool is currently restricted to operation in two dimensions, a simulation zone was extracted from the overall flow path (see Figure 21) to ensure that the sensors could be continuously simulated along the flow path as accuracy falls sharply once the regression methodology goes from interpolation to extrapolation. With this in mind it was important to ensure that sensor location are not selected too far along the flow path as the downstream sensor has the potential to be located outside of the interpolation volume. Similarly to the evolution of the flow distribution as a function of flow rate found in Figure 17 above, it is also of particular interest to investigate a similar evolution at various points along the flow path itself as shown in Figures 22 and 23. The extent of the flow rate evolution acts to confirm the validity of an investigation into the evolution of the application of ATF sensors at varying distributions along the flow path.

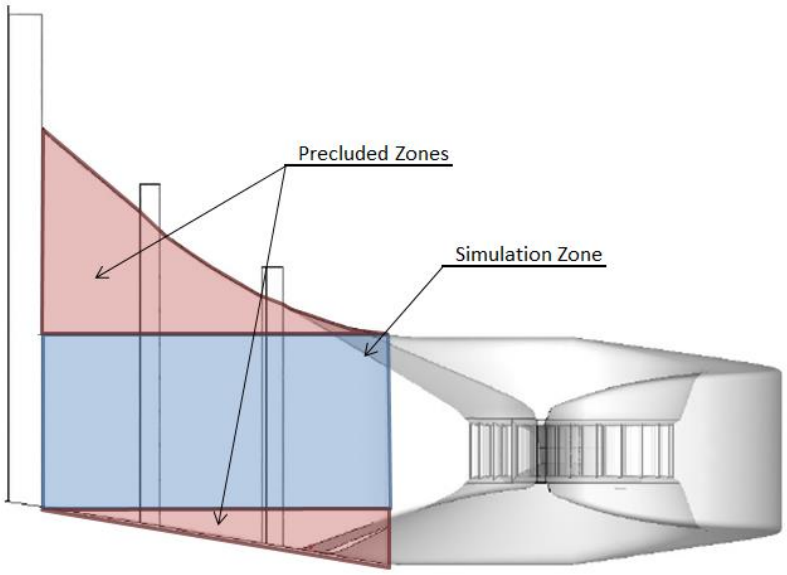

Figure 21: Flow Path Constraint

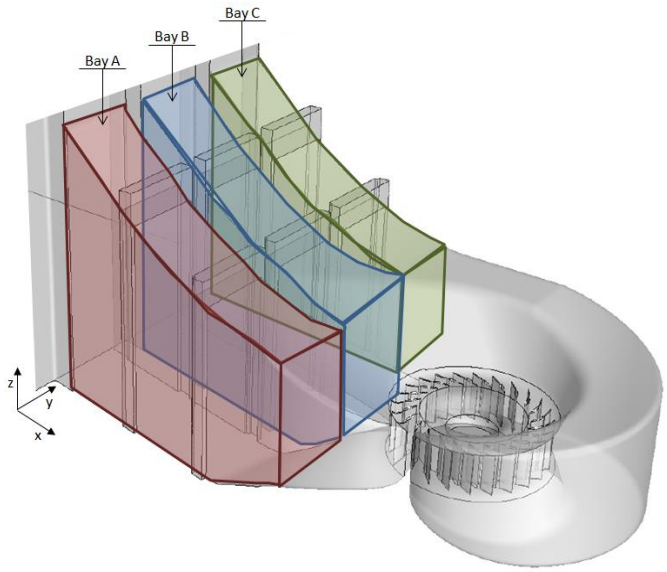

Figure 22: Bay Determination

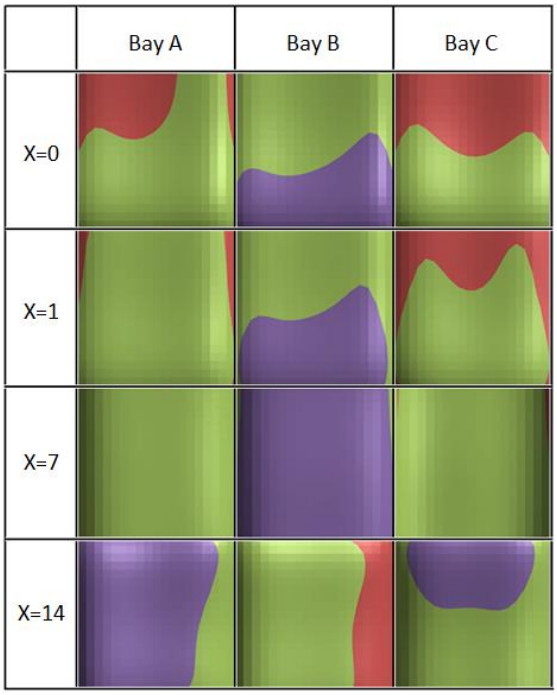

Figure 23: Velocity Transects

An investigation was performed to determine the performance of the sensors at: the entrance, one foot downstream, and seven feet downstream. This study demonstrated several of the interesting attributes of the flow that this tool is specifically designed to quantify. Firstly it can be seen that the flow rate is largely skewed towards Bay C with the recorded flow rates being: 46.24±4.26; 63.3±5.55; and 87.36±6.92 ft^3sec^{-1} for Bays: A, B and C respectively. It is suspected by the author that this is a result of the intake design itself, because the flow path from Bay into the scroll case becomes increasingly impeded as can be seen in Figure [24]. Conformation of this statement requires analysis of a statistically significant number of additional intakes. This tool, however, is designed to facilitate the rapid analysis of data required to do this and therefore this represents further work for the author.

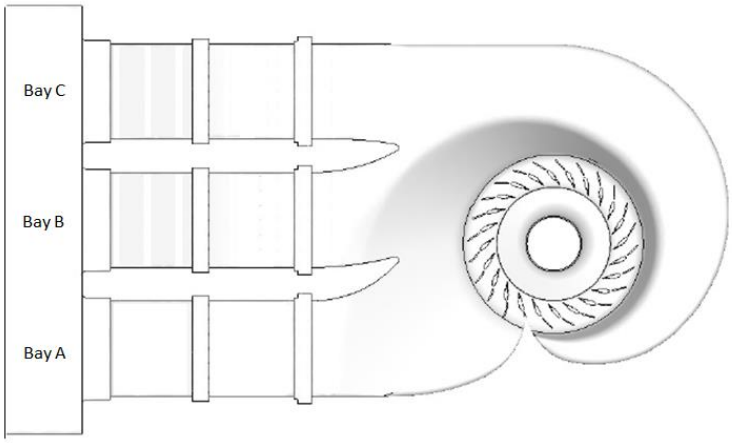

Figure 24: Case Study Geometry

Further analysis of the data demonstrates several interesting facts, the first of which is the evolution of the accuracy of the sensors in the three Intake Bays as their placement depth increases (found in Figures 25 through 27). As a clarification it should be noted by the reader that in the Figures the horizontal axis refers to the placement of the upstream sensor. It can be seen consistently that the highest accuracy consistently occurs when the downstream sensor is located 3 ft downstream and the lowest accuracy is located 7 ft downstream. The rationale behind these variances is investigated by analyzing the cross sectional velocity distribution at the midpoint of the acoustic path (where 5.795 and 9.795 are the midpoints of upstream sensor locations of 3 and 7 respectively). It can be seen that a higher average axial velocity (v) will result in a larger disparity between the double acoustic path and the single acoustic path. Additionally a higher standard deviation is more likely to result in variation between the measured velocities as can be seen from Table [1]. These statements are not conceptually novel, however the ability to rapidly quantify the variability from ideal conditions and the resulting impact on accuracy that this causes very much is. Aside from this the full results of this case study can be observed in the tables found in Section 9.2 below.

Table 1: Bay A-C Transect Characteristics

		Bay A		Bay B		Bay C	
		Average	Stand Dev	Average	Stand Dev	Average	Stand Dev
5.795 ft	u	1.21236	0.0856	1.655	0.1146	2.27	0.1547
	v	0.0012	0.02038	0.0033	0.0288	0.0018	0.0399
9.795 ft	u	1.3982	0.12	1.8926	0.15951	2.59	0.2059
	v	0.02155	0.01484	0.03476	0.0175	0.011	0.0082

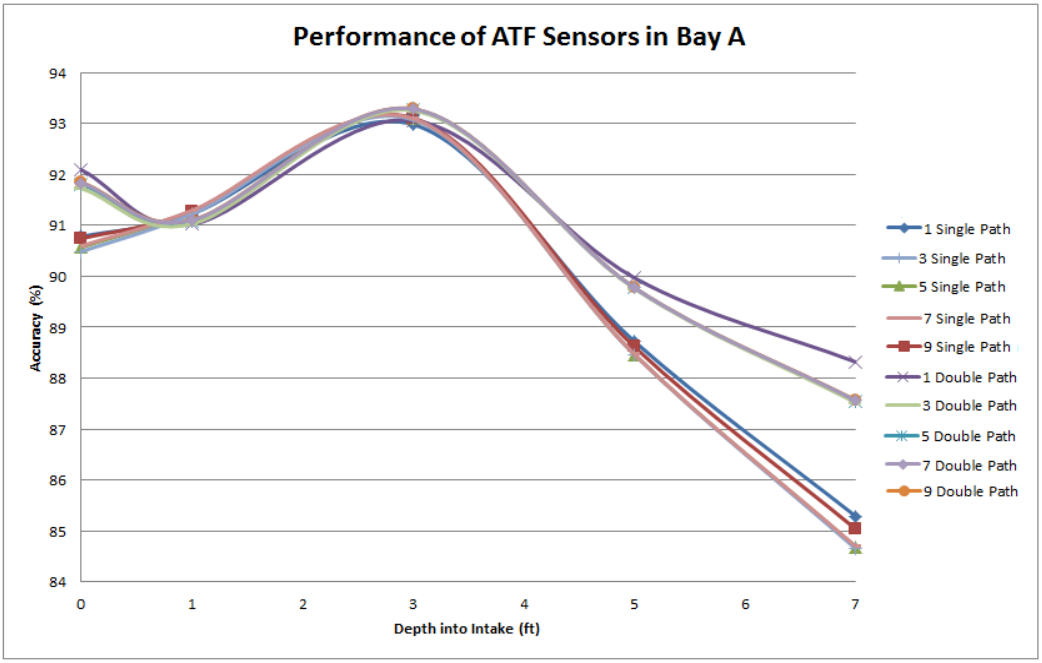

Figure 25: Bay A Sensor Performance Based on Application Depth

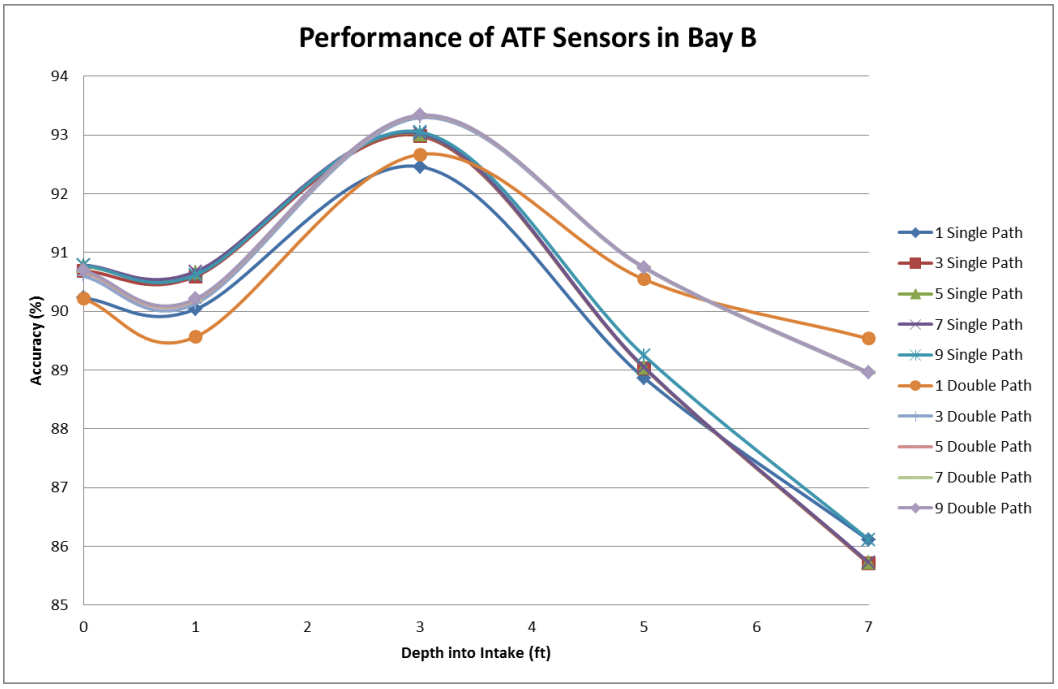

Figure 26: Bay B Sensor Performance Based on Application Depth

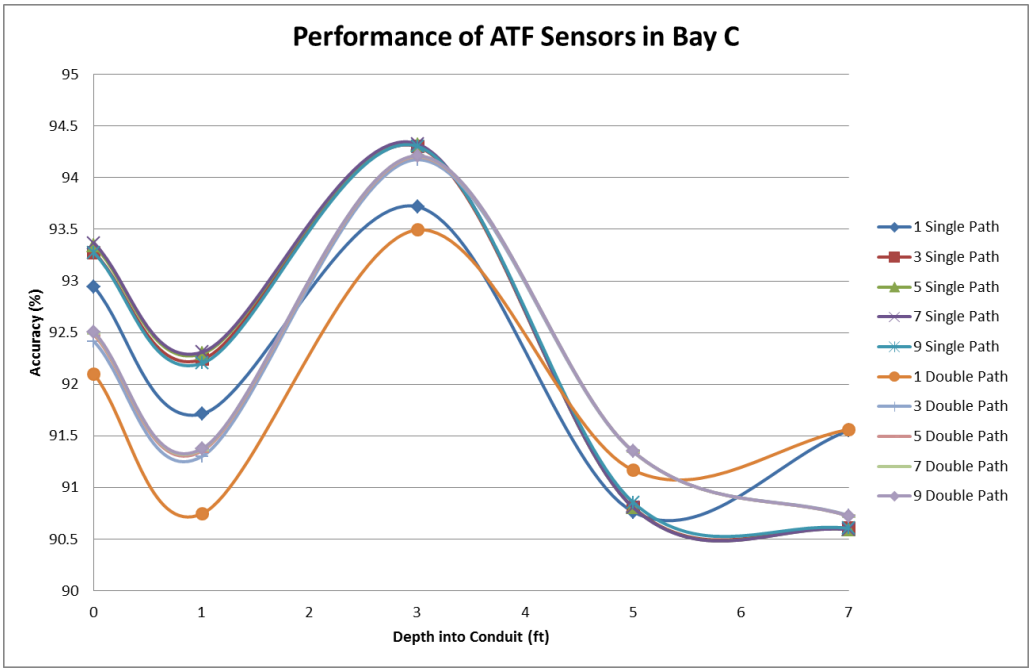

Figure 27: Bay C Sensor Performance Based on Application Depth

8.0 Appendix: Operational Instructions

This section is included to provide the user with step-by-step instructions for the operation of both the Current Meter and Acoustic Time of Flight Simulation tools provided. The tools are each comprised of two discrete subsections: the Regression and Simulation Sections. These address conversion of the field data to an overall function and determination of the flow rates predicted by varying numbers of sensors

respectively. Given its numerical complexity the Regression Section is comprised of two discrete Matlab codes for the 2 and 3 Dimensional Regressions. It should be noted by the reader that successful operation of the code requires the Symbolic Math optional toolkit. Similarly the Sensor Simulation section of the tool is comprised of two Microsoft Excel Files. The decision was made to develop this section of the tool with Excel to broaden the applicability of the overall tool.

8.1 Regression Subsection

The following section is designed to provide the reader with instruction to convert point velocity measurements to a function the flow rate across the measurement section.

8.1.1 Data Configuration

Configuration of the data is of crucial importance to the successful operation of the tool. The data should be placed in a Microsoft Excel file arranged as demonstrated in Tables 2 and 3 for the Current Meter and Acoustic Time of Flight regressions respectively. It is important for the reader to understand the both variation that exists in the dimensional assignments between the two and three dimensional tools and the requirement of the data dimensions to be positive. In the case of the two dimensional regression x and y coordinates refer to the breadth and height of the conduit respectively, whereas in the three dimensional regression x, y and z coordinates refer to the streamwise length, the breadth and the height of the conduit. The reader is referred to Figures 12 and 14 above which visually address this variation. As per operational requirements of Matlab, the files that are processed must be located in the same file as the regression code and the name of the excel file should not contain spaces. The locational data is required (specifically for the three dimensional regression of the ATF simulation) because of the conversion from the Cartesian coordinate system to a path length coordinate system. If the locational data is negative it introduces the possibility of negative and positive mathematical roots. While this does not necessarily preclude the conversation it requires a level of user interaction that detracts from the ease of use of this tool. As a clarification it should be noted that the positive requirement does not apply in any way to the velocity data inputted.

Table 2: CM Data Input Layout

X	Y	U
X-1 Location	Y-1 Location	U-1 Location
X-2 Location	Y-2 Location	U-2 Location
…	…	…
X-n Location	Y-n Location	U-n Location

Table 3: ATF Data Input Layout

X	Y	Z	U	V	W
X-1 Location	Y-1 Location	Z-1 Location	U-1 Location	V-1 Location	W-1 Location
X-2 Location	Y-2 Location	Z-2 Location	U-2 Location	V-2 Location	W-2 Location
…	…	…	…	…	…
X-n Location	Y-n Location	Z-n Location	U-n Location	V-n Location	W-n Location

8.1.2 Matlab Code Operation

This section will address the two specific areas that must be adjusted by the user of the tool the: file name of the data to be processed and the order of the polynomial that is to be regressed. As demonstrated in Figures 28 and 29 the file name of the data to be read in is found on lines 19 and 18 for the two dimensional and three dimensional regressions respectively (boxed in red). It is important to note that the filename, complete with extension, should be bracketed by apostrophes as they are already in the file.

The order of the polynomial regression is then selected by the user by a simply changing the number in the code at the appropriate place, line 27 and 30 for the two and three dimensional codes respectively. The appropriate locations are demonstrated in Figure 28 and 29 (boxed in blue). It should be noted by the reader that the subsequent Excel file only has the capacity to address regressions up to the 6th order and therefore at preset to this value.

```
1     %Mark Christian
2     %10/13/14
3     %3D Regression Code
4     %
5     %This work is performed in support of Mark Christian's
6     %Hydro Research Foundation Fellowship
7     %
8     %House Keeping Functions
9 -   clc
10 -  clear all
11 -  close all
12
13    %Reading in Location and Velocity Values
14    %Structured in X-Y-Z-U-V-W
15    %================DATA FILE READ IN and Process==================
16 -  filename = 'Data File.xlsx'; %File name of data to be analyzed
17    %Data Extract
18 -  data = xlsread(filename);
19 -  lenght = size(data);
20 -  lenght_dataset = lenght (1,1);
21 -  x_values = data (1:lenght_dataset,1);
22 -  y_values = data (1:lenght_dataset,2);
23 -  z_values = data (1:lenght_dataset,3);
24 -  u_values = data (1:lenght_dataset,4);
25 -  v_values = data (1:lenght_dataset,5);
26 -  w_values = data (1:lenght_dataset,6);
27
28    %==================Polynomial Regression=======================
29    %Subset 1: Generation of the Regression Maxtrises
30 -  Polynomial Order = 6; %This is the order of the polynomial that models
31                          %the data
```

Figure 28: 2D Regression Code Data Entry

```
%Mark Christian
%March 19th 2014
%2D Regression Analysis Code

%This work is performed in support of Mark Christian's
%

%{
Note that additional information for the Numerical Method can be found at:
http://reliawiki.org/index.php/Multiple_Linear_Regression_Analysis
%}

%---------------------------House Keeping Functions
clc
clear all
close all

%------------DATA FILE READ IN AND PROCESSING-----------------------------
filename = 'Data File.xlsx' %File name of data to be analyzed

%Data Extract
data = xlsread(filename);
dimentions=size(data);
length=dimentions(1);

%------------CONTROLLED ITEMS----------------
Order of Polynomial= 6%<-Toggels the Order of the Polynomial
stepsize=.5;%Stepsize Controls the Resolution of the Graph of the Produced Function

%--------Calculates the X/Y Sum Data
```

Figure 29: 3D Regression Code Data Entry

8.1.3 Matlab Code Results

The following section describes the results of both the two and three dimensional regression codes. In both cases the code results in the desired coefficients for the polynomial. In the case of the three dimensional code they are labeled: “U_Coefficients”, “V_Coefficients”, and “W_Coefficients” whereas in the two dimensional code they are simply “Coefficients”. These values are extremely important as they will need to be transported into the Excel tool for analysis. The Matlab code also provides the user with information as to the accuracy of the regression technique both through the calculation of the average error and through a visual comparison. The average error is calculated by assessing the function produced through the regression at the points where data was provided and comparing it to said data. This is done at every point provided, and the average (in 1 and 3 directions depending on the tool used) is provided to the user. Visual comparison is then provided to the user for both the two and three dimensional regression as seen in Figures 30 and 31. In the two dimensional regression the velocity function surface is graphed along with the provided data points (shown as red circles). In the three dimensional regression the velocity vectors of the provided data is compared to the results predicted by the function at those same points. Given the potential data density the decision was made to not overlay these two graphs.

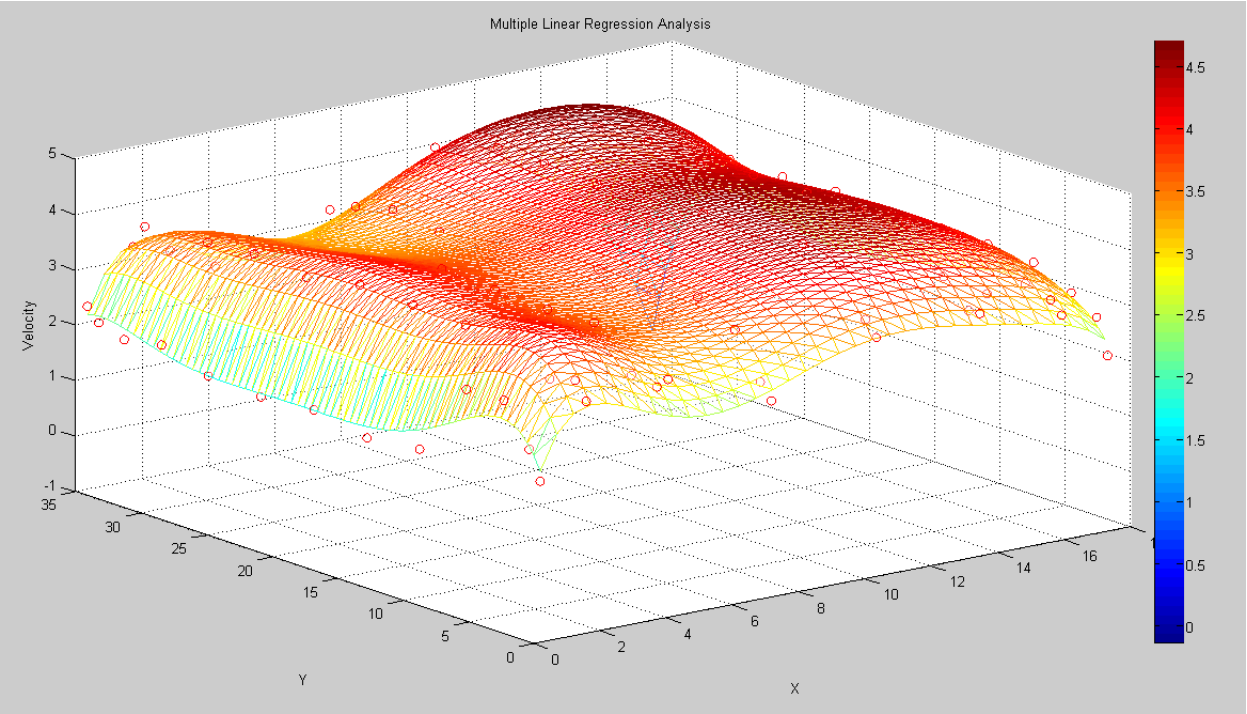

Figure 30: 2D Regression Code Visual Confirmation

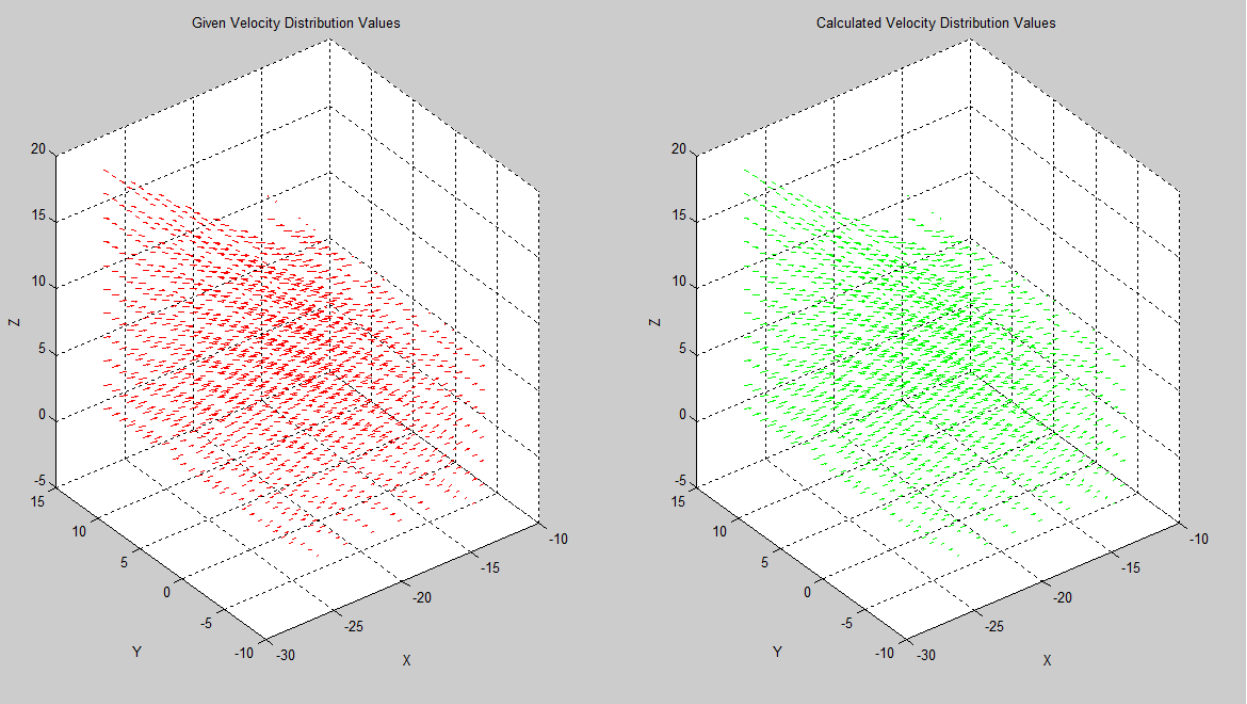

Figure 31: 3D Regression Code Visual Confirmation

8.2 Sensor Simulation Subsection

The following section will address the utilization of the excel tools for the simulation of the sensors at varying levels. The specifics of how the sensors themselves is addressed in the appropriate sections above. Each individual section addresses both the data that the user is required to enter along with the important data that is produced by the tool in turn.

8.2.1 Current Meter Simulation

8.2.1.1 Data Entry

While using the Current Meter Simulation Excel Tool there are two pieces of information that must be inputted by the user for accurate operation of the tool. The first is the entry of the conduit dimensions in the appropriate locations; this area is boxed in blue in Figure 32. It should be noted that the maximum and minimum locations of the sensors should not be used; rather the outer dimensions of the conduit should be used. The second set of information that must be entered are the coefficients calculated by the two dimensional Matlab regression software. It should be noted by the reader that if a regression less than a 6^{th} order is used, the higher order coefficients should be replaced with zeros.

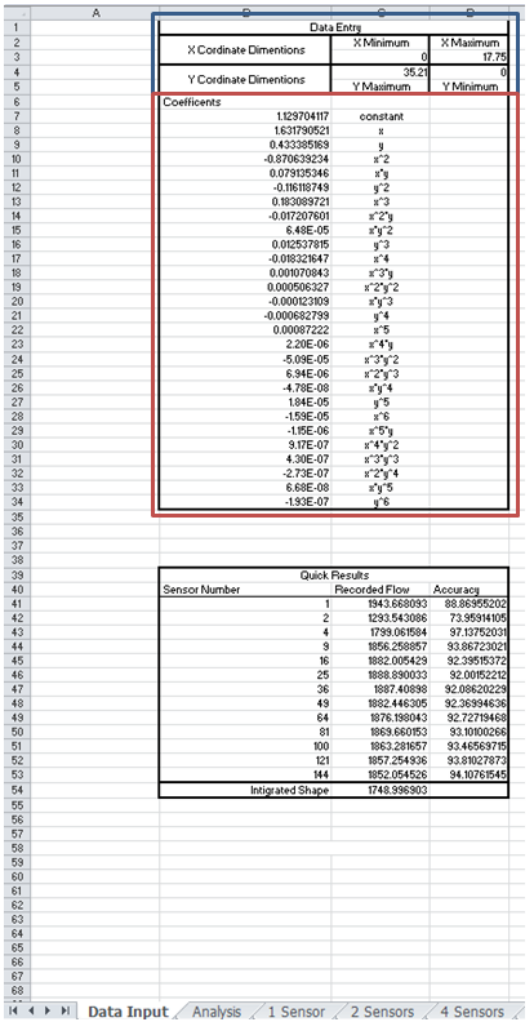

Data Entry		
X Cordinate Dimentions	X Minimum	X Maximum
	0	17.75
Y Cordinate Dimentions	35.21	0
	Y Maximum	Y Minimum

Coefficents	
1.129704117	constant
1.631790521	x
0.433385169	y
-0.870639234	x^2
0.079135346	x*y
-0.116118749	y^2
0.183089721	x^3
-0.017207601	x^2*y
6.48E-05	x*y^2
0.012537815	y^3
-0.018321647	x^4
0.001070843	x^3*y
0.000506327	x^2*y^2
-0.000123109	x*y^3
-0.000682799	y^4
0.00087222	x^5
2.20E-06	x^4*y
-5.09E-05	x^3*y^2
6.94E-06	x^2*y^3
-4.78E-08	x*y^4
1.84E-05	y^5
-1.59E-05	x^6
-1.15E-06	x^5*y
9.17E-07	x^4*y^2
4.30E-07	x^3*y^3
-2.73E-07	x^2*y^4
6.68E-08	x*y^5
-1.93E-07	y^6

Quick Results		
Sensor Number	Recorded Flow	Accuracy
1	1943.668093	88.86955202
2	1293.543086	73.95914105
4	1799.061584	97.13752031
9	1856.258857	93.86723021
16	1882.005429	92.39515372
25	1888.890033	92.00152212
36	1887.40898	92.08620229
49	1882.446305	92.36994636
64	1876.198043	92.72719468
81	1869.660153	93.10100266
100	1863.281657	93.46569715
121	1857.254936	93.81027873
144	1852.054526	94.10761545
Intigrated Shape	1748.996903	

Figure 32: Current Meter Simulation Data Entry

8.2.1.2 Data Produced

The Current Meter Simulation Excel file produces three discrete pieces of data useful for the user: a visualization of the flow profile; the evolution of the flow rate based on the number of sensors; and the evolution of the accuracy of the flow measurement system based on the number of sensors. The visualization of the velocity distribution is primarily used as a method to quickly confirm the accuracy of the data entered, however it also acts as a convent visualization of the velocity distribution. This was found to be particularly useful, as it allows for a quick diagnosis of the accuracy of the overall system. This is found on the first workbook of the tool and is shown in Figure 33. The flow rate indicated per sensor applied is both provided and graphed along with the variation that exists in the accuracy of the predicted flow rate based on the number of sensors. These are boxed in green, purple and orange respectively in Figure 34.

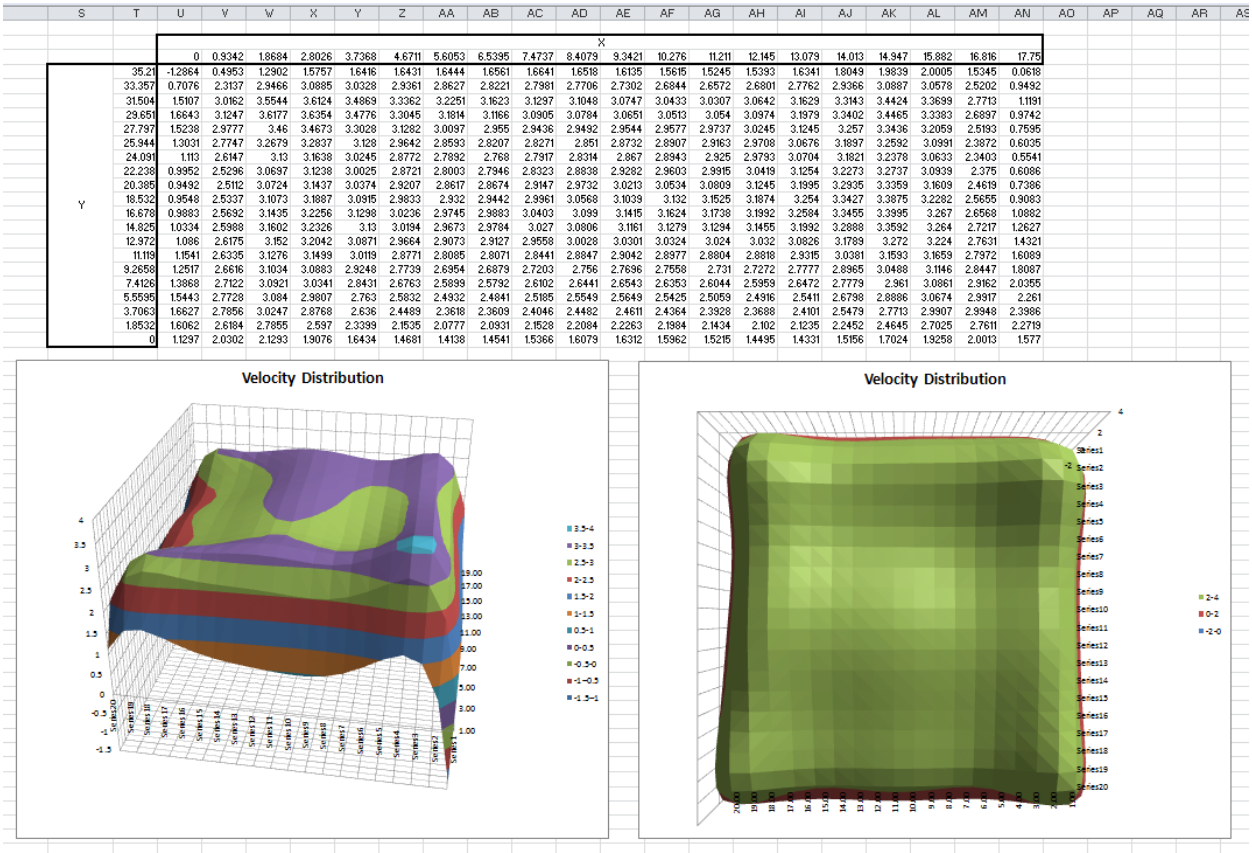

		X																								
		0	0.9342	1.8684	2.8026	3.7368	4.6711	5.6053	6.5395	7.4737	8.4079	9.3421	10.276	11.211	12.145	13.079	14.013	14.947	15.882	16.816	17.75						
Y	35.21	-1.2864	0.4953	1.2902	1.5757	1.6416	1.6431	1.6444	1.6561	1.6641	1.6518	1.6135	1.5615	1.5245	1.5393	1.6341	1.8049	1.9839	2.0005	1.5345	0.0618						
	33.357	0.7076	2.3137	2.9466	3.0885	3.0328	2.9361	2.8627	2.8221	2.7981	2.7706	2.7302	2.6844	2.6572	2.6801	2.7762	2.9366	3.0887	3.0578	2.5202	0.9492						
	31.504	1.5107	3.0162	3.5544	3.6124	3.4869	3.3362	3.2251	3.1623	3.1297	3.1048	3.0747	3.0433	3.0307	3.0642	3.1629	3.3143	3.4424	3.3699	2.7713	1.1191						
	29.651	1.6643	3.1247	3.6177	3.6354	3.4776	3.3045	3.1814	3.1166	3.0905	3.0784	3.0651	3.0513	3.054	3.0974	3.1979	3.3402	3.4465	3.3383	2.6897	0.9742						
	27.797	1.5238	2.9777	3.46	3.4673	3.3028	3.1282	3.0097	2.955	2.9436	2.9492	2.9544	2.9577	2.9737	3.0245	3.1245	3.257	3.3436	3.2059	2.5193	0.7595						
	25.944	1.3031	2.7747	3.2679	3.2837	3.128	2.9642	2.8593	2.8207	2.8271	2.851	2.8732	2.8907	2.9163	2.9708	3.0676	3.1897	3.2592	3.0991	2.3872	0.6035						
	24.091	1.113	2.6147	3.13	3.1638	3.0245	2.8772	2.7892	2.768	2.7917	2.8314	2.867	2.8943	2.925	2.9793	3.0704	3.1821	3.2378	3.0633	2.3403	0.5541						
	22.238	0.9952	2.5296	3.0697	3.1238	3.0025	2.8721	2.8003	2.7946	2.8323	2.8838	2.9282	2.9603	2.9915	3.0419	3.1254	3.2273	3.2737	3.0939	2.375	0.6086						
	20.385	0.9492	2.5112	3.0724	3.1437	3.0374	2.9207	2.8617	2.8674	2.9147	2.9732	3.0213	3.0534	3.0809	3.1245	3.1995	3.2935	3.3359	3.1609	2.4619	0.7386						
	18.532	0.9548	2.5337	3.1073	3.1887	3.0915	2.9833	2.932	2.9442	2.9961	3.0568	3.1039	3.132	3.1525	3.1874	3.254	3.3427	3.3875	3.2282	2.5655	0.9083						
	16.678	0.9883	2.5692	3.1435	3.2256	3.1298	3.0236	2.9745	2.9883	3.0403	3.099	3.1415	3.1624	3.1738	3.1932	3.2584	3.3455	3.3995	3.267	2.6568	1.0882						
	14.825	1.0334	2.5988	3.1602	3.2326	3.13	3.0194	2.9673	2.9784	3.027	3.0806	3.1161	3.1279	3.1294	3.1455	3.1992	3.2888	3.3592	3.264	2.7217	1.2627						
	12.972	1.086	2.6175	3.152	3.2042	3.0871	2.9664	2.9073	2.9127	2.9558	3.0028	3.0301	3.0324	3.024	3.032	3.0826	3.1789	3.272	3.224	2.7631	1.4321						
	11.119	1.1541	2.6335	3.1276	3.1499	3.0119	2.8771	2.8085	2.8071	2.8441	2.8847	2.9042	2.8977	2.8804	2.8818	2.9315	3.0381	3.1593	3.1659	2.7972	1.6089						
	9.2658	1.2517	2.6616	3.1034	3.0883	2.9248	2.7739	2.6954	2.6879	2.7203	2.756	2.7696	2.7558	2.731	2.7272	2.7777	2.8965	3.0488	3.1146	2.8447	1.8087						
	7.4126	1.3868	2.7122	3.0921	3.0341	2.8431	2.6763	2.5899	2.5792	2.6102	2.6441	2.6543	2.6353	2.6044	2.5959	2.6472	2.7779	2.961	3.0861	2.9162	2.0355						
	5.5595	1.5443	2.7728	3.084	2.9807	2.763	2.5832	2.4932	2.4841	2.5185	2.5549	2.5649	2.5425	2.5059	2.4916	2.5411	2.6798	2.8886	3.0674	2.9917	2.261						
	3.7063	1.6627	2.7856	3.0247	2.8768	2.636	2.4489	2.3618	2.3609	2.4046	2.4482	2.4611	2.4364	2.3928	2.3688	2.4101	2.5479	2.7713	2.9907	2.9948	2.3986						
	1.8532	1.6062	2.6184	2.7855	2.597	2.3399	2.1535	2.0777	2.0931	2.1528	2.2084	2.2263	2.1984	2.1434	2.102	2.1235	2.2452	2.4645	2.7025	2.7611	2.2719						
	0	1.1297	2.0302	2.1293	1.9076	1.6434	1.4681	1.4138	1.4541	1.5366	1.6079	1.6312	1.5962	1.5215	1.4495	1.4331	1.5156	1.7024	1.9258	2.0013	1.577						

Figure 33: Current Meter Velocity Distribution Visualization

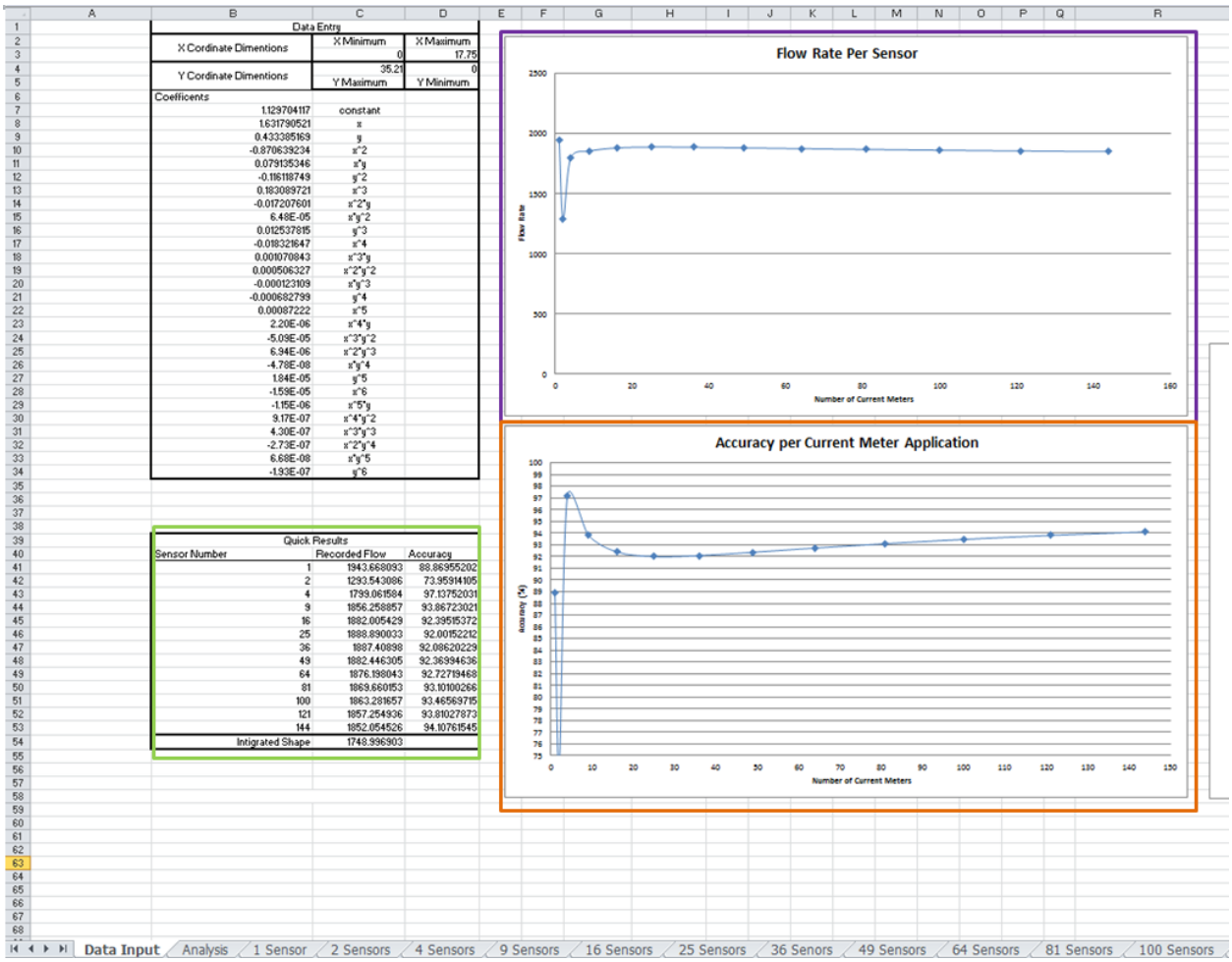

Figure 34: Current Meter Simulation Results

8.2.2 Acoustic Time of Flight Simulation

8.2.2.1 Data Entry

As with the CM data entry section above there are two primary sets of data that must be entered; the geometry of the conduit and the regression coefficients calculated by the three dimensional Regression Matlab Code. Naturally given the three dimensional nature of this tools a higher level of information must be provided. This can been seen in Figure 35 where geometrical data for the conduit in question must be provided in three dimensions in the area boxed in blue (remembering the variation in the coordinate system as described above). The area boxed in red in Figure 35 represents the location within the ATF simulation tool where the coefficients for the velocity in three directions must be entered. There is an increase in the number of coefficient terms from 28 to 83 as a result of the change from a two to a three dimensional regression.

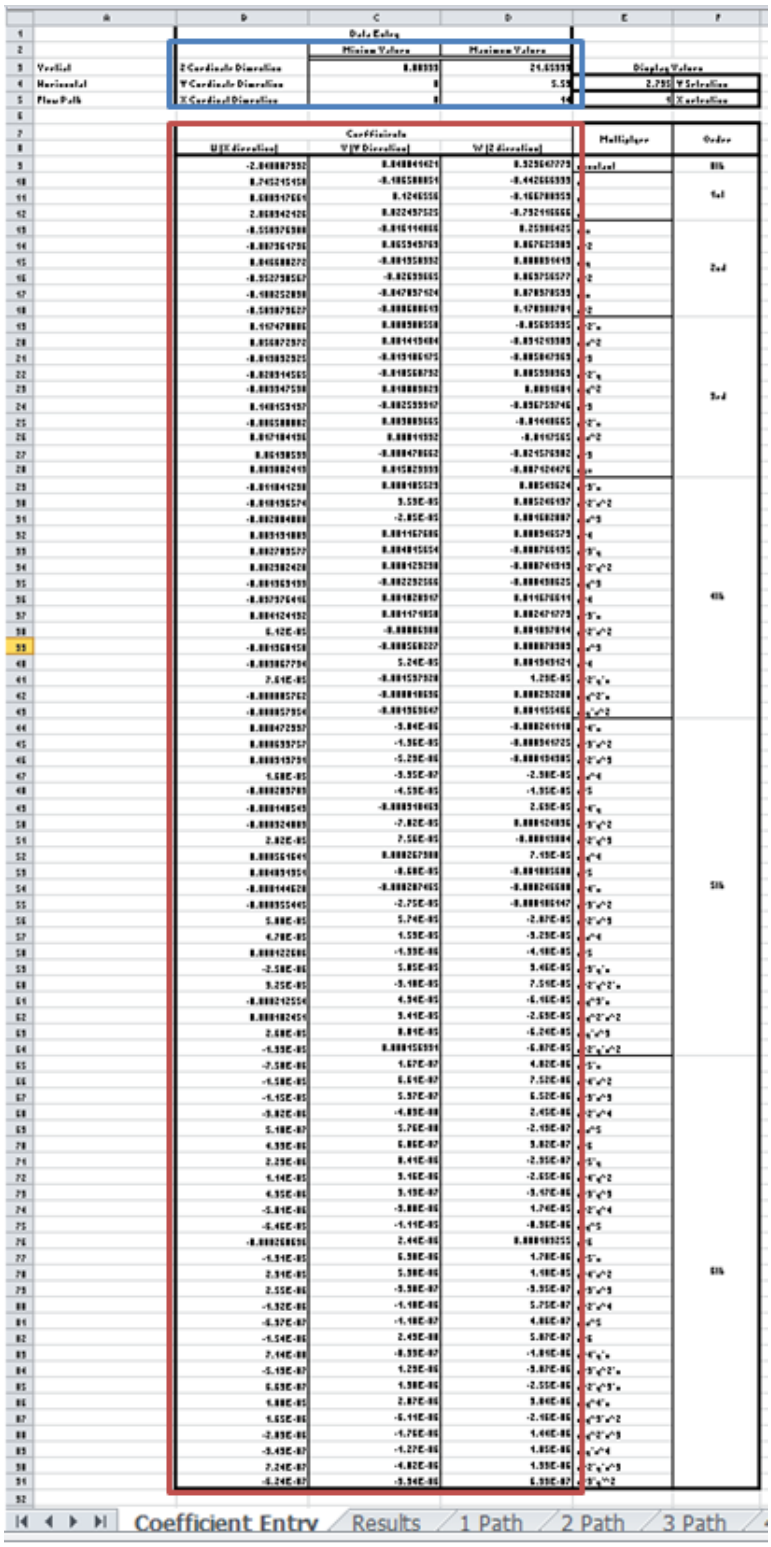

Figure 35: ATF Simulation Tool Data Entry

8.2.2.2Data Provided

As with the CM tool, the ATF simulation tool provides the user information as to the distribution of the flow, the change in indicated flow rate based on the number of sensors applied and the evolution of the accuracy of the flow measurement system as the number of sensors increases. Visualization of the velocity distribution, as before, is an extremely useful tool to indicate the accuracy of the sensor prediction tool. Given the three dimensional nature of the velocity distribution, the user needs to select the plane (x and y) in which the velocity will be visualized. The plane selection location is boxed in pink in Figure 36 (found in the top left), and this controls the visualization of the velocity distribution of U at a constant streamwise location (boxed in yellow) and the velocity distribution of V as a constant location in the width (boxed in blue). This information is found in the first workbook, labeled “Coefficient Entry”, of the ATF simulation tool. In the “Results” workbook of the ATF tool the numerical the evolution of both the indicated flow rate (boxed in brown) and the accuracy thereof (boxed in teal) is presented as shown in Figure 37.

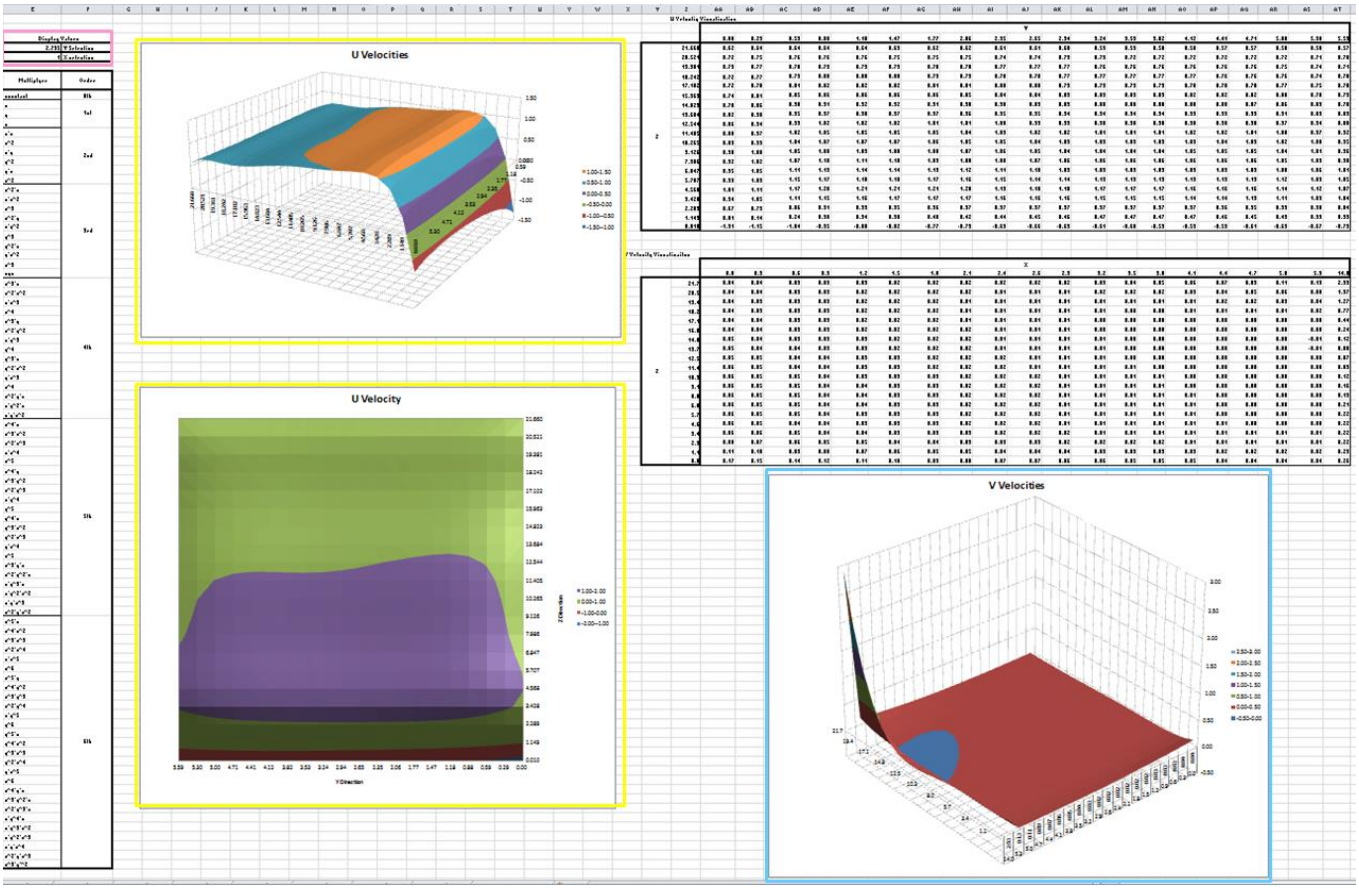

Figure 36: Acoustic Time of Flight Velocity Distribution Visualization

Figure 37: ATF Results Section

9.0 Appendix: Case Study Data

9.1 Current Meter Case Study Data

Table 4: Bay A CM Sensor Simulation Results

	Bay A							
	Run 1		Run 2		Run 3		Run 4	
Sensor Number	Recorded Flow	Accuracy	Recorded Flow	Accuracy	Recorded Flow	Accuracy	Recorded Flow	Accuracy
1	1954.656486	86.944621	2866.458334	85.29635	3156.675861	87.2433	3835.50453	86.35074
2	1459.946703	84.441859	1903.85451	76.18428	2294.417462	81.9567	3048.492362	90.32942
4	1813.23554	95.124267	2666.166766	93.31118	2981.10076	93.5149	3618.482049	92.7813
9	1858.164784	92.525605	2715.441136	91.33942	3037.313745	91.507	3683.114977	90.86617
16	1876.460296	91.46741	2732.136262	90.67135	3055.07755	90.8724	3701.78483	90.31297
25	1878.943871	91.323763	2729.866236	90.76219	3052.070248	90.9798	3695.893866	90.48752
36	1874.724883	91.567785	2720.073411	91.15406	3041.014601	91.3748	3680.724621	90.937
49	1867.965681	91.95873	2707.853092	91.64306	3027.440175	91.8596	3662.856696	91.46644
64	1860.483709	92.39148	2695.340735	92.14376	3013.63317	92.3528	3644.970552	91.99642
81	1853.066025	92.820512	2683.399203	92.62161	3000.504242	92.8218	3628.105431	92.49615
100	1846.040176	93.22688	2672.340465	93.06413	2988.374174	93.2551	3612.60406	92.95547
121	1839.52449	93.603741	2662.236262	93.46846	2977.308923	93.6503	3598.513029	93.373
144	1833.959731	93.925601	2653.556452	93.81579	2967.869174	93.9875	3587.07969	93.71178
Integrated Shape	1728.937182	100	2499.012215	100	2799.546885	100	3374.861009	100

Table 5: Bay B CM Sensor Simulation Results

	Bay B							
	Run 1		Run 2		Run 3		Run 4	
Sensor Number	Recorded Flow	Accuracy	Recorded Flow	Accuracy	Recorded Flow	Accuracy	Recorded Flow	Accuracy
1	2197.980608	91.837951	3157.628938	91.75593	3511.474195	94.1803	4366.629449	90.92478
2	1870.140577	92.029127	2688.192192	92.15169	1906.605913	57.4563	4101.210835	97.55475
4	2135.727244	94.901423	3071.812211	94.69775	3471.224786	95.3933	4220.152071	94.58368
9	2163.952042	93.512488	3109.84122	93.39411	3563.464206	92.6136	4270.03491	93.33764
16	2170.91402	93.169891	3118.220251	93.10687	3591.87842	91.7573	4281.408049	93.05355
25	2167.669949	93.329531	3112.628921	93.29854	3591.797526	91.7597	4273.783051	93.24402
36	2160.771961	93.668979	3102.174842	93.65691	3580.995566	92.0853	4259.444679	93.60218
49	2152.921176	94.055314	3090.568258	94.05479	3566.704137	92.5159	4243.480884	94.00094
64	2145.182589	94.436128	3079.248508	94.44283	3551.849249	92.9636	4227.884032	94.39054
81	2137.951189	94.791983	3068.733272	94.80329	3537.5978	93.3931	4213.377856	94.7529
100	2131.344249	95.117109	3059.162547	95.13138	3524.374926	93.7916	4200.162706	95.083
121	2125.364236	95.411384	3050.522931	95.42755	3512.28694	94.1558	4188.224917	95.3812
144	2120.585996	95.64652	3043.491223	95.6686	3501.777385	94.4725	4178.612885	95.6213
Integrated Shape	2032.118133	100	2917.138165	100	3318.356614	100	4003.319526	100

Table 6: Bay C CM Sensor Simulation Results

	Bay C							
	Run 1		Run 2		Run 3		Run 4	
Sensor Number	Recorded Flow	Accuracy	Recorded Flow	Accuracy	Recorded Flow	Accuracy	Recorded Flow	Accuracy
1	2563.932573	89.227594	3582.038119	90.22435	4066.364489	87.1756	4866.032824	87.53191
2	1128.205055	48.743087	1192.242459	36.53763	2819.767664	78.2366	968.2598384	22.37928
4	2493.598257	92.266325	3461.401785	93.92139	3760.654146	95.6578	4613.800796	93.36173
9	2524.363151	90.937156	3522.125689	92.06043	3833.058259	93.6489	4683.081653	91.76044
16	2527.899706	90.784362	3538.628228	91.55469	3864.324503	92.7814	4702.048693	91.32206
25	2519.371461	91.152817	3533.643876	91.70744	3868.699606	92.66	4694.071133	91.50645
36	2507.041746	91.685511	3520.741196	92.10286	3861.417499	92.862	4676.049025	91.92299
49	2494.163531	92.241903	3505.58088	92.56747	3849.650819	93.1885	4655.23671	92.40402
64	2481.935982	92.770183	3490.435119	93.03163	3836.574916	93.5513	4634.567052	92.88176
81	2470.74465	93.253695	3476.174525	93.46866	3823.578918	93.9119	4615.159509	93.33032
100	2460.652736	93.689707	3463.081053	93.86992	3811.247394	94.254	4597.368097	93.74153
121	2451.599857	94.080829	3451.188489	94.23438	3799.795753	94.5718	4581.224282	94.11466
144	2444.913687	94.369699	3441.975095	94.51674	3789.731176	94.851	4566.877308	94.44626
Integrated Shape	2314.59501	100	3263.053365	100	3604.154019	100	4326.589891	100

9.2 Acoustic Time of Flight Case Study

Table 7: Bay A ATF Sensor Simulation Results

		0.00001				1				7			
	Number of Sensors	Flow Rate		Flow Rate Accuracy (%)		Flow Rate		Flow Rate Accuracy (%)		Flow Rate		Flow Rate Accuracy (%)	
		Single Path	Double Path	Single Path	Double Path	Single Pat	Double Path	Single Pat	Double Path	Single Path	Double Path	Single Path	Double Path
Bay A	1	47.48718434	46.91790629	90.78053995	92.08986671	47.95898	48.05012714	91.22993	91.02321481	58.67672191	57.1286095	85.29380681	88.3201872
	2	47.66217883	47.11980308	90.37805654	91.62550862	47.99393	48.08102373	91.15068	90.95314194	59.01459076	57.54017387	84.63331235	87.51562655
	3	47.6151703	47.07594723	90.4861751	91.7263761	47.96205	48.04743057	91.22298	91.02933059	59.0028954	57.53539168	84.65617543	87.52497517
	4	47.5911444	47.05286227	90.54143415	91.77947097	47.94635	48.03103313	91.25858	91.06651968	58.9916094	57.5260007	84.67823824	87.54333346
	5	47.57862722	47.04075103	90.57022337	91.80732656	47.93822	48.02256065	91.27702	91.08573509	58.98505575	57.520231	84.69104987	87.55461255
	6	47.57145026	47.03378661	90.58673022	91.82334458	47.93357	48.01771697	91.28757	91.09672046	58.98113594	57.51671221	84.69871265	87.56149137
	7	47.56699313	47.02945489	90.59698153	91.83330742	47.93068	48.01471304	91.29412	91.10353332	58.97864879	57.5144584	84.70357474	87.56589732
	8	47.56404779	47.02658986	90.60375574	91.83989693	47.92877	48.01272953	91.29845	91.10803188	58.97698447	57.51294212	84.70682828	87.56886147
	9	47.5037759	47.02460115	90.74237973	91.84447092	47.94062	48.01135417	91.27158	91.11115118	58.80536424	57.51187816	85.04232595	87.57094139
	Intigrated Result:	43.4786844				44.09207618				51.15392663			

Table 8: Bay B ATF Sensor Simulation Results

		0.00001				1				7			
	Number of Sensors	Flow Rate		Flow Rate Accuracy (%)		Flow Rate		Flow Rate Accuracy (%)		Flow Rate		Flow Rate Accuracy (%)	
		Single Path	Double Path	Single Path	Double Path	Single Pat	Double Path	Single Pat	Double Path	Single Path	Double Path	Single Path	Double Path
Bay B	1	65.62437174	65.63096721	90.22398786	90.21295501	66.45376	66.73858448	90.0359	89.56459624	79.38470099	76.99565506	86.10623799	89.53381819
	2	65.42127658	65.46410096	90.56372409	90.49208775	66.17938	66.45588003	90.48994	90.03240031	79.66842122	77.4016475	85.69918267	88.95133812
	3	65.34822169	65.40129433	90.68592982	90.59715027	66.11646	66.3969361	90.59405	90.12993752	79.6651804	77.41001544	85.70383231	88.93933257
	4	65.31777638	65.37466416	90.73685854	90.64169704	66.09129	66.37352678	90.63571	90.168674	79.65766857	77.40571901	85.71460959	88.9454967
	5	65.30273974	65.36143216	90.76201172	90.66383144	66.07899	66.36211365	90.65606	90.18755984	79.65298329	77.4023719	85.72133158	88.95029882
	6	65.29431174	65.3539946	90.77611002	90.67627293	66.07213	66.35575114	90.66741	90.19808818	79.65010834	77.40018391	85.72545629	88.95343794
	7	65.28913988	65.34942337	90.78476149	90.68391965	66.06793	66.35185773	90.67435	90.20453078	79.64826101	77.39873717	85.72810667	88.95551358
	8	65.28574651	65.34642122	90.79043789	90.68894164	66.06518	66.34930742	90.6789	90.20875089	79.64701582	77.39774649	85.72989316	88.95693492
	9	65.29243498	65.3443468	90.77924947	90.69241171	66.10153	66.34754822	90.61877	90.21166192	79.37825478	77.39704367	86.11548642	88.95794326
	Intigrated Result:	59.78024749				60.43223659				69.70065752			

Table 9: Bay C ATF Sensor Simulation Results

		0.00001				1				7			
	Number of Sensors	Flow Rate		Flow Rate Accuracy (%)		Flow Rate		Flow Rate Accuracy (%)		Flow Rate		Flow Rate Accuracy (%)	
		Single Path	Double Path	Single Path	Double Path	Single Path	Double Path	Single Path	Double Path	Single Path	Double Path	Single Path	Double Path
Bay C	1	89.04799879	89.74957835	92.94224224	92.09876978	90.47602507	91.28264366	91.71282	90.74741008	103.4005993	103.3913002	91.55416881	91.56392168
	2	88.85917615	89.56936252	93.16925383	92.31543386	90.10956267	90.89280539	92.15142437	91.2139921	104.248994	104.1391745	90.66437835	90.77955623
	3	88.77067654	89.48774338	93.27565229	92.41356029	90.03468602	90.81874449	92.24104128	91.30263266	104.3055873	104.1839461	90.60502372	90.73260015
	4	88.73221338	89.45222409	93.32189455	92.45626327	90.00442532	90.78929454	92.27725912	91.33788015	104.3144378	104.189306	90.59574129	90.72697872
	5	88.71295687	89.43442994	93.34504565	92.47765626	89.98956826	90.77491066	92.29504094	91.35509565	104.3164719	104.1898437	90.59360797	90.72641481
	6	88.70209636	89.42439086	93.35810266	92.48972572	89.98125749	90.7668835	92.30498777	91.36470303	104.3170152	104.1896063	90.59303822	90.72666377
	7	88.69540915	89.41820826	93.36614234	92.49715873	89.9761621	90.76196826	92.31108624	91.37058589	104.3171491	104.1892806	90.59289774	90.72700533
	8	88.69101249	89.41414287	93.37142822	92.50204633	89.97282049	90.75874728	92.31508568	91.37444095	104.3171575	104.1889952	90.59288893	90.72730468
	9	88.77386448	89.41133155	93.2718196	92.50542624	90.0669777	90.75652482	92.20239264	91.37710094	104.3042424	104.1887657	90.60643424	90.72754541
	Intigrated Result:	83.1775302				83.55192653				95.34769403			

10. Works Cited

Almquist, C., Taylor, J., & Walsh, J. (2011). Kootenay Canal Flow Rate Measurement Comparison Test Using Intake Methods. *HydroVision* , (pp. 1-17). Sacramento.

Fornberg, B., & Zuev, J. (2007). The Runge Phenomenon and Spatially Variable Shape Parameters in RBF Interpolation. *Journal of Computational and Applied Mathmatics*.

González Salgado, D., Vich Llobet, J., Muciaccia, F., Grego, G., Clarke, M., & Lemon, D. (2013). Turbine acceptance tests at Frieira HPP, Miño River, Spain with Acoustic Scintillation Flow Meter and Current Meters., (pp. 1-9). Denver.

Gruber, & Peter. (2010). Acoustic Time of Flight Measurement in the Penstock. *Hydro 2010.* Lissabon: International Journal on Hydropower & Dams.

Rittmeyer. (2014). *RISONIC Flow Sensors*. Retrieved from Instrumentation: http://www.rittmeyer.com/en/products-and-solutions/instrumentation/flow-sensors.html

Staubli, T. (1988). Propeller-type Current Meters. *Dischage and Velocity Measurement*, 95-100.

United States Department of the Interior: Bureau of Reclamation. (2001). Current Meters. In U. S. Reclamation, *Water Measurement Manual.* Washington D.C.: U.S. Government Printing Office.

For overall questions please contact:

Mark Christian

Energy Science and Engineering Doctoral Candidate

University of Tennessee and Oak Ridge National Laboratory

(865)241-8238

christianmh@ornl.gov